RSC Advances

PAPER

View Article Online
View Journal | View Issue

Cite this: *RSC Adv.*, 2024, **14**, 37521

Design, CTAB-catalyzed ultrasound-assisted synthesis and tyrosinase inhibition potential of naphthofuran-triazole conjugates†

Aqsa Mushtaq,[a] Mirza Nadeem Ahmad, *[b] Ameer Fawad Zahoor, *[a] Shagufta Kamal,[c] Kulsoom Ghulam Ali,[a] Jamila Javid,[d] Bushra Parveen,[a] Usman Nazeer[e] and Mashooq Ahmad Bhat *[f]

The development of novel and efficient tyrosinase inhibitors is a critical necessity of agricultural, cosmetic and medicinal chemistry. Bearing in mind the therapeutical potential of naphthofuran-containing organic compounds, we carried out the CTAB-catalyzed ultrasound-assisted synthesis of a library of novel naphthofuran-triazole joined *N*-aryl/alkyl acetamides **20(a–j)** in 74–92% yield, which were further assessed for their tyrosinase inhibitory potential by taking kojic acid and ascorbic acid as standard inhibitors. The tyrosinase inhibitory assay demonstrated the promising tyrosinase inhibiting tendency of all prepared derivatives **20(a–h)** as they all were found to be more efficient in comparison to the standard kojic acid. Similarly, most of the derivatives also exhibited tyrosinase inhibition potency in juxtaposition to ascorbic acid. More specifically, among the catalog of compounds, **20f** and **20i** exhibited potent inhibition results with $IC_{50} = 0.51 \pm 0.12$ and 1.99 ± 0.07, respectively. Overall, **20f** was shown to be the most efficacious tyrosinase inhibitor, owing to the presence of an electronegative group, *i.e.*, 2-chloro substitution on the phenyl ring. The tyrosinase inhibition activity results of **20f** and **20i** were further supplemented with molecular docking analysis to validate experimental studies. *In silico* modelling findings revealed their significant interactions with the tyrosinase protein (PDB ID: 5OAE), thereby illustrating the efficient docking score of −7.10 kcal mol^{-1} and −6.95 kcal mol^{-1} in comparison to kojic acid (−5.03 kcal mol^{-1}).

Received 4th August 2024
Accepted 10th November 2024

DOI: 10.1039/d4ra05649c

rsc.li/rsc-advances

1. Introduction

Various plants, microorganisms and animals are known to possess copper-containing metalloenzymes, *i.e.*, tyrosinase, which is responsible for the synthesis of polyphenolic compounds, melanin and neuromelanin.[1–3] In insects, the tyrosinase enzyme is involved in the hardening of cuticles and invasion-triggered encapsulation.[4] Monophenols are hydroxylated and *o*-quinones are obtained from *o*-diphenols in the presence of the tyrosinase enzyme, to synthesize melanin.[5–8] Melanin is involved in the pigmentation and color templates of mammalian skin. Furthermore, melanin also guards the skin from harmful sun radiation.[9] Several dermatological complications originate from the anomalous decline of melanin.[10] In a similar manner, many skin problems (*i.e.*, senile lentigines, cervical poikiloderma, melasma, acanthosis nigricans and freckles) arise as a result of excessive production of melanin and aggregation of pigmentation.[11] Moreover, studies have confirmed that the excess tyrosinase activity results in neurodegenerative diseases, *i.e.*, Parkinson's disease among mammals[12] and skin cancer high-risk factors.[13] In addition, unrestrained activity of the tyrosinase enzyme leads to immense browning in fruits and vegetables. As a result, the quality and trade value of these fruits and vegetables severely suffer.[14–16] These conditions highlight the requirement of efficient tyrosinase inhibitors.

To date, various natural and synthetic tyrosinase inhibitors have been shown to suppress or reduce the extravagant activity of the tyrosinase enzyme. Some examples of natural tyrosinase inhibitors include kojic acid, arbutin, kaempferol, cuminaldehyde and glabrene. Similarly, dopastin, tropolone, cupferron and 4-hexylresourcinol are some examples of synthetic tyrosinase inhibitors.[17] However, only arbutin and kojic acid are

[a]*Department of Chemistry, Government College University Faisalabad, Faisalabad 38000, Pakistan. E-mail: fawad.zahoor@gcuf.edu.pk*

[b]*Department of Applied Chemistry, Government College University Faisalabad, Faisalabad 38000, Pakistan. E-mail: pioneeravian@hotmail.com*

[c]*Department of Biochemistry, Government College University Faisalabad, Faisalabad 38000, Pakistan*

[d]*Department of Chemistry, University of Sialkot, Sialkot, Pakistan*

[e]*Department of Chemistry, University of Houston, 3585 Cullen Boulevard, Texas 77204-5003, USA*

[f]*Department of Pharmaceutical Chemistry, College of Pharmacy, King Saud University, Riyadh 11451, Saudi Arabia. E-mail: mabhat@ksu.edu.sa*

† Electronic supplementary information (ESI) available. See DOI: https://doi.org/10.1039/d4ra05649c

harnessed in medicinal and cosmetic industry. These inhibitors have some uninviting side effects, *i.e.*, mutagenesis, DNA alterations, malignancy induction and other susceptibilities.[18–20] In order to minimize the dreadful aspects of excessive tyrosinase activity, researchers are continuously trying to develop novel and efficient tyrosinase inhibitors.[21–27]

Naphthofuran-based derivatives are of impeccable significance owing to their wide biological potential.[28–30] Organic compounds incorporated with naphthofuran scaffolds are known to be highly effective against several ailments, *i.e.*, bacterial,[31] viral[32] and fungal diseases.[33] These scaffolds have also been ascertained to be active against diabetes[34] and inflammatory diseases.[35] These also act as efficient antioxidant[36] and pain-relieving agents.[37] Various natural products are endowed with the naphthofuran moiety and exhibit potent pharmacological applications. For example, the naphthofuran-substituted naturally occurring organic compound, *i.e.*, NFD (naphtho[1,2-*b*]furan-4,5-dione) **1** was originally obtained from *Avicennia marina*. NFD was revealed as a potent anti-tumour agent that displayed anti-proliferative activities against the human cervical, hepatocellular and epidermoid cancer cell lines.[38] Similarly, rubicordifolin **2**,[39] (+)-heritol **3**,[40–42] (+)-laevigatin **4**[43] and balsaminone A **5**[44] are some other examples of naturally occurring naphthofuran-constituting organic compounds, which are highly acclaimed as significant pharmacological and anti-cancer agents (Fig. 1).

The pharmacological activity of various naphthofuran derivatives has been significantly explored by researchers to reveal their therapeutic efficacy. Nitro-based naphthofurans have also been extensively investigated for their mutagenic potential.[45] These functionalized scaffolds are also utilized as effective NF-κβ, *i.e.*, nuclear transcription factor kappa-β inhibitors and IKK-β (inhibitory kappa β-kinase) inhibitors.[28] The naphthofuran-based sulfonamides **6** & **7** have been discovered to be efficacious agents against TNBC (triple-negative breast cancer)[46] (Fig. 2). Many naphthofuran derivatives have also proven themselves to be promising tyrosinase inhibitors[28] (Fig. 2).

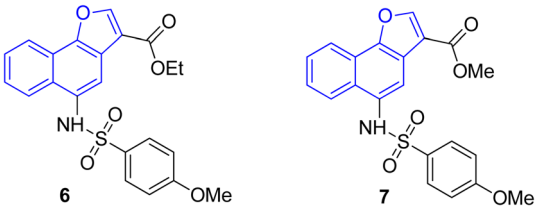

Fig. 2 Structures of biologically active naphthofuran derivatives.

Several nitrogen and oxygen containing heterocyclic scaffolds have become quintessential in the development of biologically active organic compounds owing to their myriad biological and medicinal applications.[47–52] Benzimidazole,[53] coumarin,[54] benzofuran,[55] thiadiazoles,[56] oxadiazole,[57] piperazine[58] and triazole[59]-based organic compounds have been observed to illustrate anti-cancer, anti-viral, anti-bacterial, anti-depressant, anti-inflammatory, anti-histaminic, anti-diabetic, anti-oxidant and analgesic properties. The combination of two or three heterocyclic frameworks has been determined to certainly aggravate their biological potential.[60,61] Considering the impact of heterocyclic hybridization approach, our research group has devoted efforts to synthesize and utilize the pharmacological potential of these nitrogen- and oxygen-constituting heterocyclic organic compounds, which were assessed to depict remarkable tyrosinase inhibition activity. Earlier, we established the synthesis and bacterial tyrosinase inhibition studies of benzofuran oxadiazoles endowed with sulfur alkylated amides **8** (ref. 62) and tosyl piperazine-based dithiocarbamates **9**.[63] We also reported the preparation and assessment of triazole-joined β-hydroxy sulfides **10** (ref. 64) and coumarin-based triazole derivatives **11** (ref. 65) as efficacious tyrosinase inhibitors (Fig. 3).

Factoring in the remarkable tyrosinase inhibition tendency of organic compounds endowed with triazole, oxadiazole and piperazine-based heterocyclic frameworks, we decided to proceed with the hybridization of biologically active fragments.

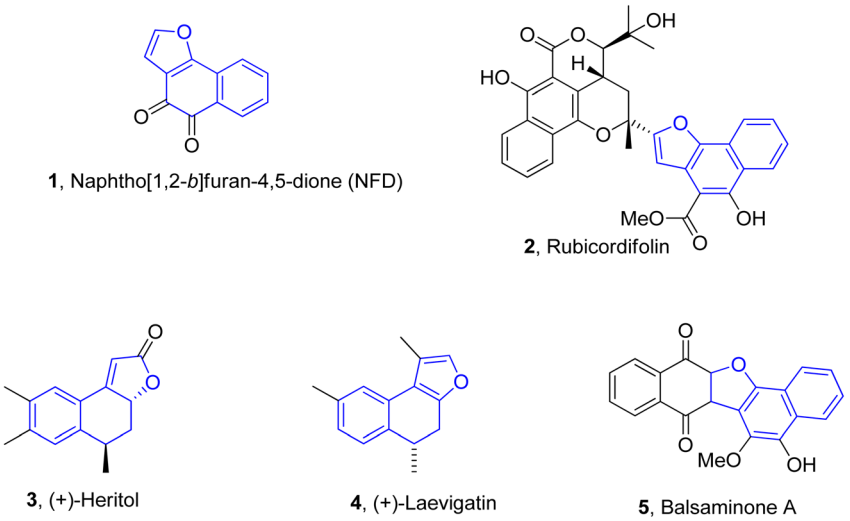

Fig. 1 Structures of naphthofuran-constituting biologically active natural products.

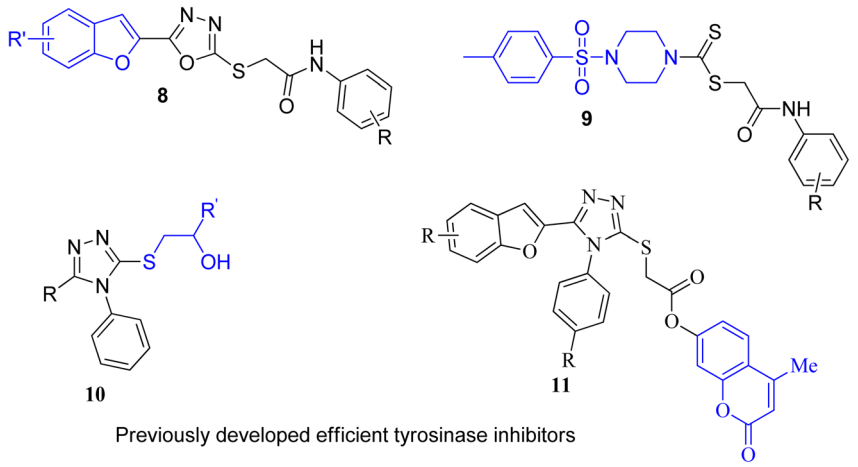

Fig. 3 Structures of previously developed efficient tyrosinase inhibitors.

We built the rationale design of developing novel naphthofuran-triazole hybrids as a result of hybridization of medicinally potent naphthofuran-based triazole ring with *N*-alkylated/arylated acetamide derivatives. The synthesized naphthofuran-triazole hybrids were further processed by ascertaining their efficacy as promising bacterial tyrosinase inhibitors (Fig. 4).

2. Results and discussion

2.1. Chemistry

The synthetic strategy of naphthofuran-based derivatives is depicted in Schemes 1–3. Reaction of commercially available 2-hydroxy-1-naphthaldehyde **12** with ethyl chloroacetate **13** using potassium carbonate in dimethylformamide at 90–95 °C furnished naphthofuran ester **14** in 75% yield.[66] The naphthofuran ester **14** was then transformed to corresponding carbohydrazide **15** (in 100% yield) on reaction with hydrazine monohydrate in methanol under reflux conditions. The synthesized naphthofuran-based carbohydrazide **15** was further converted to respective triazole scaffold **16** (in 77% yield) on treatment with phenylisothiocyanate in dichloromethane followed by nucleophilic cyclization by exploiting 2 N NaOH solution and distilled water under reflux conditions[67] (Scheme 1).

The synthesized naphthofuran-based triazole **16** was then subjected to nucleophilic substitution reaction with substituted bromo-acetanilides **19(a–j)** (obtained by treating substituted amines/anilines **18(a–j)** with bromoacetyl bromide **17** (ref. 68) (Scheme 2)) *via* two routes. One pathway involved the conventional route utilizing potassium carbonate as a base in DMF solvent[68] to access the target molecules in 56–80% yield. The second route was proceeded with the catalytic addition of CTAB

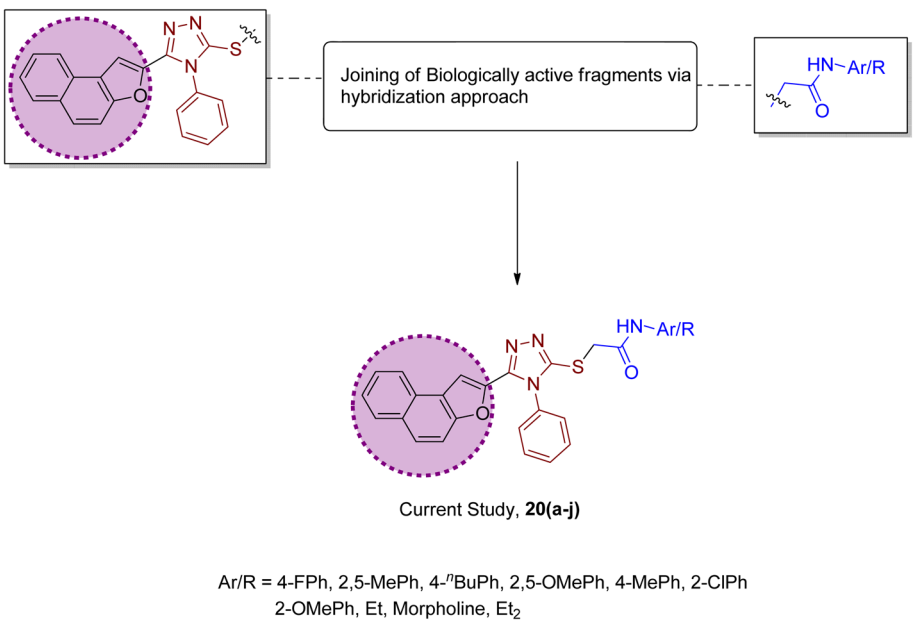

Fig. 4 Rational design of the novel naphthofuran triazole–acetamide hybrids **20(a–j)**.

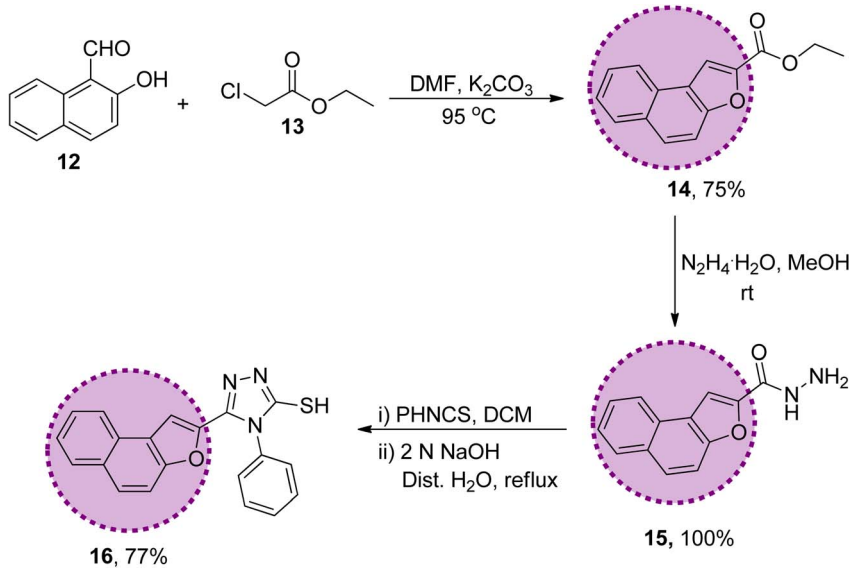

Scheme 1 Synthesis of the naphthofuran-based-triazole precursor **16**.

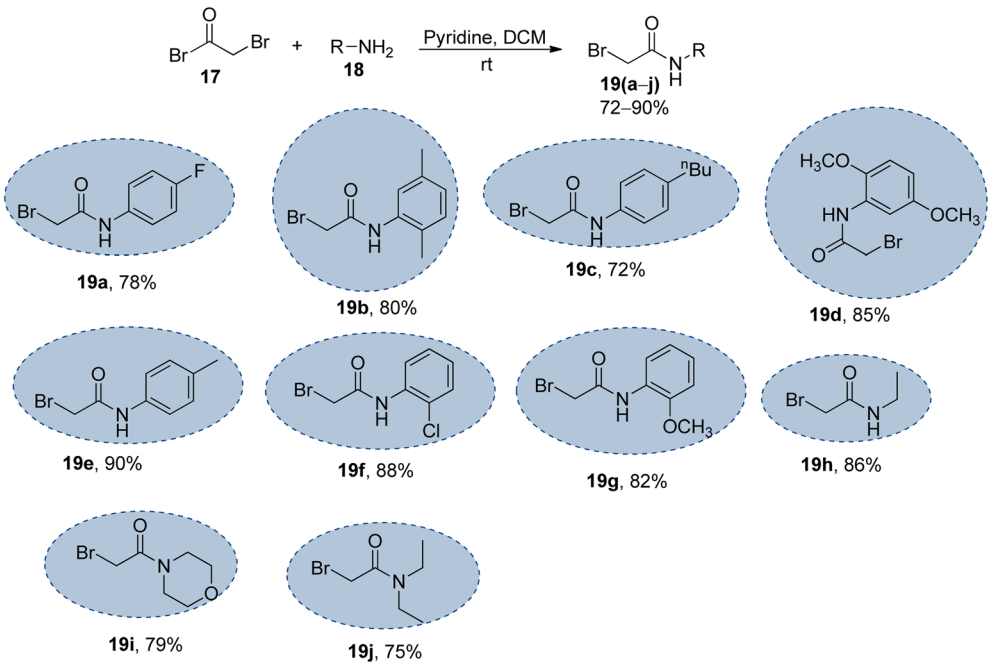

Scheme 2 Synthesis of the bromo-acetanilide/acetamide precursors **19(a–j)**; **17** (1.2 equiv.), **18** (1.0 equiv.), pyridine (1.2 equiv.).

(cetyltrimethylammonium bromide) and potassium iodide in dimethylformamide under sonication conditions, which afforded the targeted naphthofuran-based triazole–acetamide hybrids **20(a–j)** in comparatively higher yields (74–92%) within a short duration (Scheme 3, Table 1).

2.2. Anti-tyrosinase activity

The synthesized naphthofuran-based derivatives were analyzed *via in vitro* assay to determine their potential astyrosinase inhibitors. The tyrosinase enzyme was originally extracted using previously reported method.[69,70] The results indicated that almost all of the synthesized compounds were found to be more potent against tyrosinase enzyme as compared to the standard, *i.e.*, ascorbic acid and kojic acid ($IC_{50} = 11.5 \pm 1.00$ & 30.34 ± 0.75) (Fig. 5). Their IC_{50} values were found to be in the range of 0.51–23.03 μM. The compound **20f** was the most potent enzyme inhibitor among all other derivatives with percentage inhibition of 32.34 ± 0.07 and $IC_{50} = 0.51 \pm 0.12$, exhibiting more potency than both standards. Moreover, the results indicated that **20i** exhibited high activity as a tyrosinase inhibitor with percentage inhibition $= 30.55 \pm 0.1$ and ($IC_{50} = 1.99 \pm 0.07$), in comparison

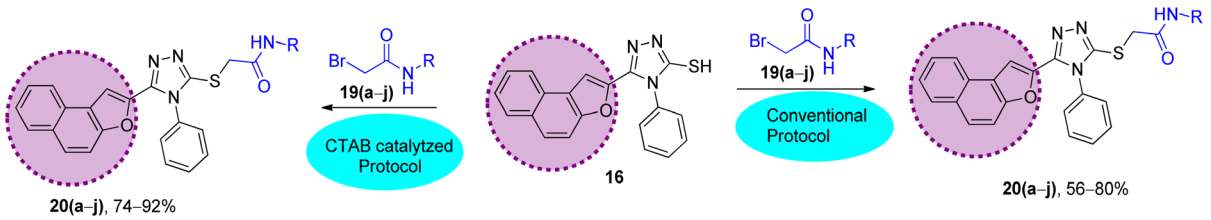

Scheme 3 Synthetic scheme to prepare the naphthofuran triazole–acetamide hybrids **20(a–j)** *via* conventional and CTAB-catalyzed protocol: (A) conventional protocol: K_2CO_3, DMF, 95 °C; (B) CTAB-catalyzed protocol (improved protocol): CTAB, K_2CO_3, KI, DMF, ultrasound, 80 °C.

with standards. Similarly, percentage inhibition of compounds **20a**, **20b**, **20c**, **20d** & **20e** was found to be in the range of 22.62–31.40 (with IC_{50} value range = 3.37 ± 0.13–5.63 ± 0.12), depicting efficient inhibitory potential than ascorbic acid and kojic acid. Among these five hybrids, **20b** displayed efficient tyrosinase inhibition (31.40 ± 0.25) with IC_{50} value of 3.37 ± 0.13 μM. Para-substituted hybrids **20a** and **20e** were observed to portray the 22.84 ± 0.05 and 4.46 ± 0.25 percentage inhibition with corresponding IC_{50} values of 4.88 ± 0.17 μM and 4.46 ± 0.25 μM. Moreover, hybrids **20c** and **20d** illustrated percentage tyrosinase inhibition of 22.62 ± 0.30 and 22.77 ± 0.17 with 5.29 ± 0.15 and 5.63 ± 0.12 μM IC_{50} values, respectively.

In a similar manner, **20h** was also found to be an effective tyrosinase inhibitor (with percentage inhibition of 13.92 ± 0.11 and IC_{50} = 9.36 ± 0.06 μM) as compared to both standards. However, the synthesized derivatives **20g** and **20j** had significantly less tyrosinase inhibition potential with percentage inhibition = 5.40 ± 0.05 & 2.61 ± 0.50, respectively. Their IC_{50} values were found to be 12.9 ± 0.15 μM and 23.03 ± 0.18 μM, respectively, indicating the trivial tyrosinase inhibition as compared to the standard, *i.e.*, ascorbic acid. However, they were found to be more potent in comparison to kojic acid. The descending order of the tyrosinase inhibition potential of synthesized hybrids and reference standards, as determined by *in vitro* assay is given as **20f** > **20i** > **20b** > **20e** > **20a** > **20c** > **20d** > **20h** > ascorbic acid > **20g** > **20j** > kojic acid, as displayed in Table 2.

Table 1 Comparison between the ultrasound-assisted CTAB catalyzed protocol and conventional protocol

		Conventional protocol		Ultrasound-assisted CTAB-catalyzed protocol	
Sr. no.	Compounds	Yield	Duration	Yield	Duration
1	**20a**	78%	18 h	84%	60 minutes
2	**20b**	56%	14 h	74%	40 minutes
3	**20c**	68%	13 h	84%	30 minutes
4	**20d**	75%	14 h	92%	50 minutes
5	**20e**	70%	16 h	88%	40 minutes
6	**20f**	58%	22 h	76%	20 minutes
7	**20g**	61%	18 h	79%	50 minutes
8	**20h**	62%	24 h	80%	30 minutes
9	**20i**	59%	12 h	77%	60 minutes
10	**20j**	64%	18 h	80%	30 minutes

2.3. Docking analysis

Compounds (**20f**, **20i**) with the most promising tyrosinase inhibition activity were selected for IFD (induced-fit docking) to authenticate the anti-tyrosinase activity. The reliability of the docking analysis was evaluated by cognate redocking. All possible types of interaction between the ligand and tyrosinase protein, *i.e.*, 5OAE, were comprehensively analyzed. The native ligand SVF was redocked in a molecular operating environment, and the self-docking result showed a root mean square

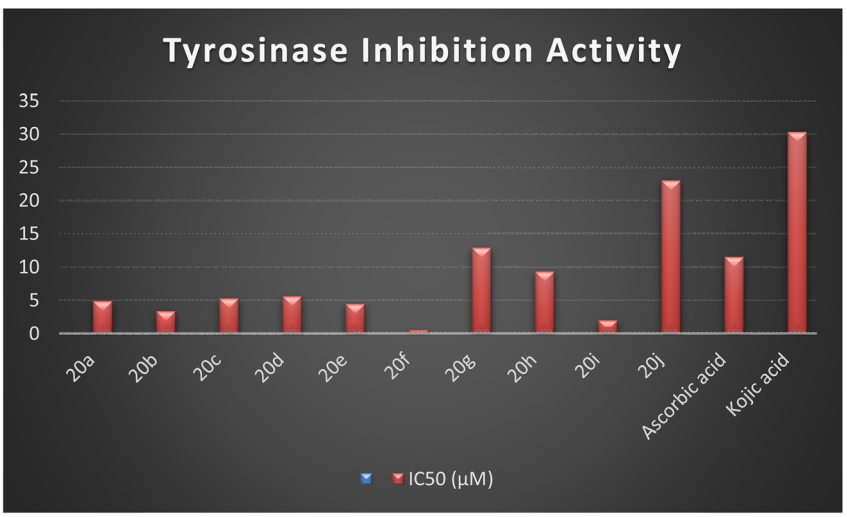

Fig. 5 Graphical illustration of the enzyme inhibition activity of the synthesized hybrids **20(a–j)** and standards.

Table 2 Tyrosinase inhibition potential of the synthesized naphthofuran triazole–acetamide hybrids **20(a–j)**

Sr. no.	Compound	Structure	Percentage inhibition	IC_{50} (μM)
1	**20a**	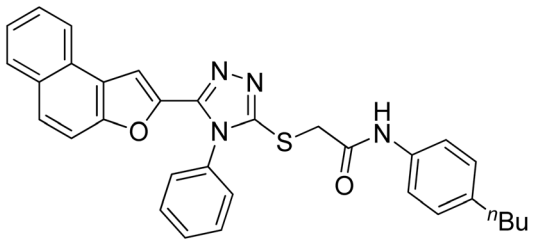	22.84 ± 0.05	4.88 ± 0.17
2	**20b**	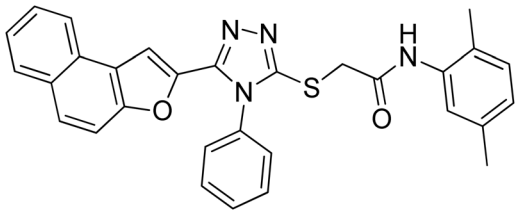	31.40 ± 0.25	3.37 ± 0.13
3	**20c**	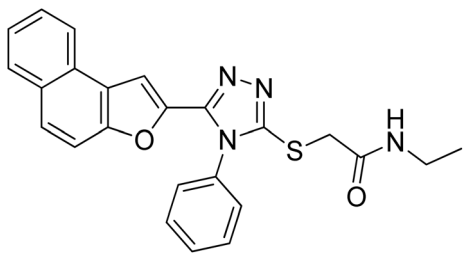	22.62 ± 0.30	5.29 ± 0.15
4	**20d**	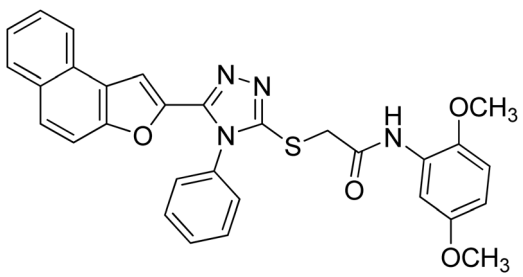	22.77 ± 0.17	5.63 ± 0.12
5	**20e**	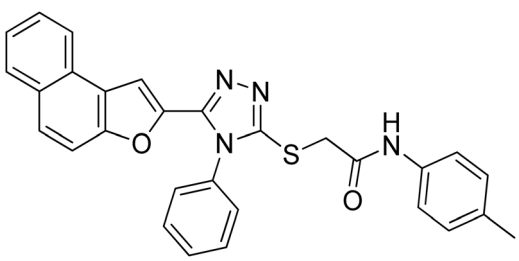	28.21 ± 0.05	4.46 ± 0.25
6	**20f**	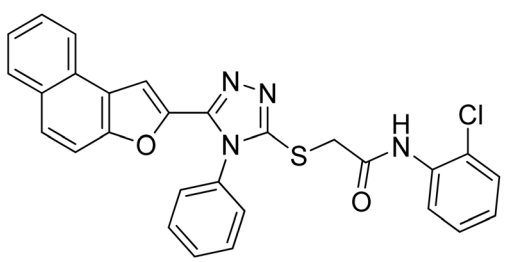	32.34 ± 0.07	0.51 ± 0.12

Table 2 (*Contd.*)

Sr. no.	Compound	Structure	Percentage inhibition	IC_{50} (μM)
7	**20g**	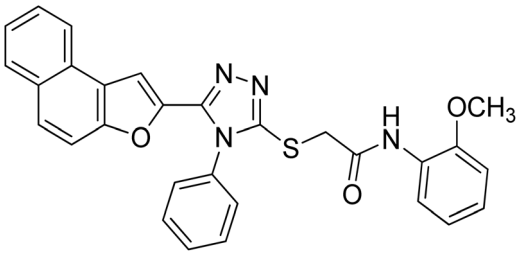	5.40 ± 0.05	12.9 ± 0.15
8	**20h**	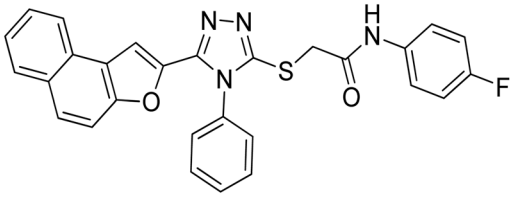	13.92 ± 0.11	9.36 ± 0.06
9	**20i**	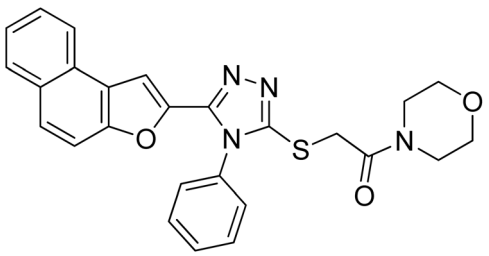	30.55 ± 0.1	1.99 ± 0.07
10	**20j**	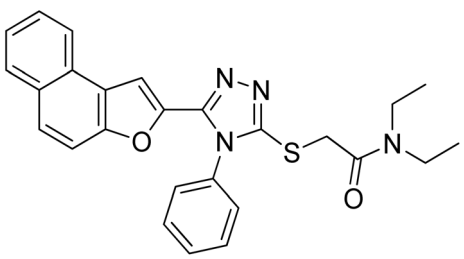	2.61 ± 0.50	23.03 ± 0.18
11	Ascorbic acid	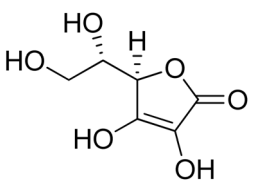	58.66 ± 1.00	11.5 ± 1.00 (ref. 50)
12	Kojic acid	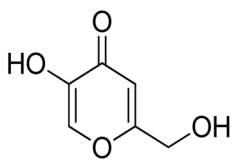	6.80 ± 0.58	30.34 ± 0.75 (ref. 50)

deviation (RMSD) value between the native ligand and redocked equal to 0.92 Å (Fig. 6).

The binding affinities of compounds (**20f** & **20i**) with the active site of the 5OAE protein were computed. Kojic acid was used as a standard IFD threshold with a binding score of ΔG −5.03 kcal mol^{-1}. The compounds (**20f** & **20i**) exhibited a higher docking score (ΔG −7.10 and −6.95 kcal mol^{-1}, respectively) than standard kojic acid, indicating their greater tyrosinase inhibitory potential (Table 3).

The protein ligand interaction study of the docked compound revealed that they interact with the receptor site around the copper core, which might be responsible for tyrosinase inhibition. It was observed that kojic acid showed both hydrophobic (VAL-218 (π–alkyl) and hydrogen bonding (GLU-

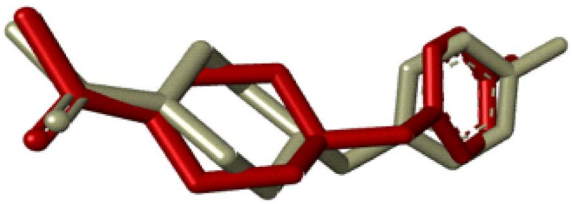

Fig. 6 IFD docking validation by RMSD between the native ligand (grey) and redocked ligand (maroon).

195, ASN-205, MET-215) interactions (Fig. 7). However, the compound **20i** showed hydrogen bonding interaction with ARG-209, GLY-200, GLU-158) and hydrophobic interactions with HIS-204, PRO-201, VAL-218, ALA-221 and pi–sulfur interaction with PHE-197 residue. However, compound (**20f**) exhibited hydrogen bonding interactions with ARG-209, PRO-201, and hydrophobic interactions with ALA-221, VAL-218 and pi–sulfur interaction with MET-184 residue.

The docking analysis inferred that the –OH group of kojic acid formed conventional H-bonding interaction with GLU-195 at 2.68 Å. Moreover, its methylene hydrogens and hydrogen atom of the pyran-one ring were observed to display carbon–hydrogen bonding interactions with MET-215 and ASN-205 at 2.75 Å and 2.65 Å, respectively. Similarly, pyran-one ring was found to portray hydrophobic interaction (π–alkyl) with VAL-218 at 4.38 Å (Fig. 7(A–C)).

However, the docking results of **20i** unveiled that its carbonyl oxygen forms conventional H-bonding with ARG-209 at 5.97 Å. Moreover, hydrogen atoms of morpholine ring were observed to be involved in carbon–hydrogen bonding interactions with GLU-158 and GLY-200 *via* 2.86 Å and 2.49 Å. Similarly, triazole

Table 3 Molecular docking scores and interactions

Compound	Binding score kcal mol^{-1}	Residue interacting with ligand	Types of interaction
Kojic acid	−5.03	ASN-205, VAL-218, GLU-195, MET-215	Hydrogen bonding, π–alkyl
20i	−6.95	GLU-158, GLY-200, PRO-201, ARG-209, PHE-197, VAL-218, HIS-204, ALA-221	Hydrogen bonding, π–sulfur, π–σ, π–π shaped, π–alkyl
20f	−7.10	MET-184, PRO-201, ARG-209, VAL-218, ALA-221	Hydrogen bonding, π–alkyl, π–sulfur

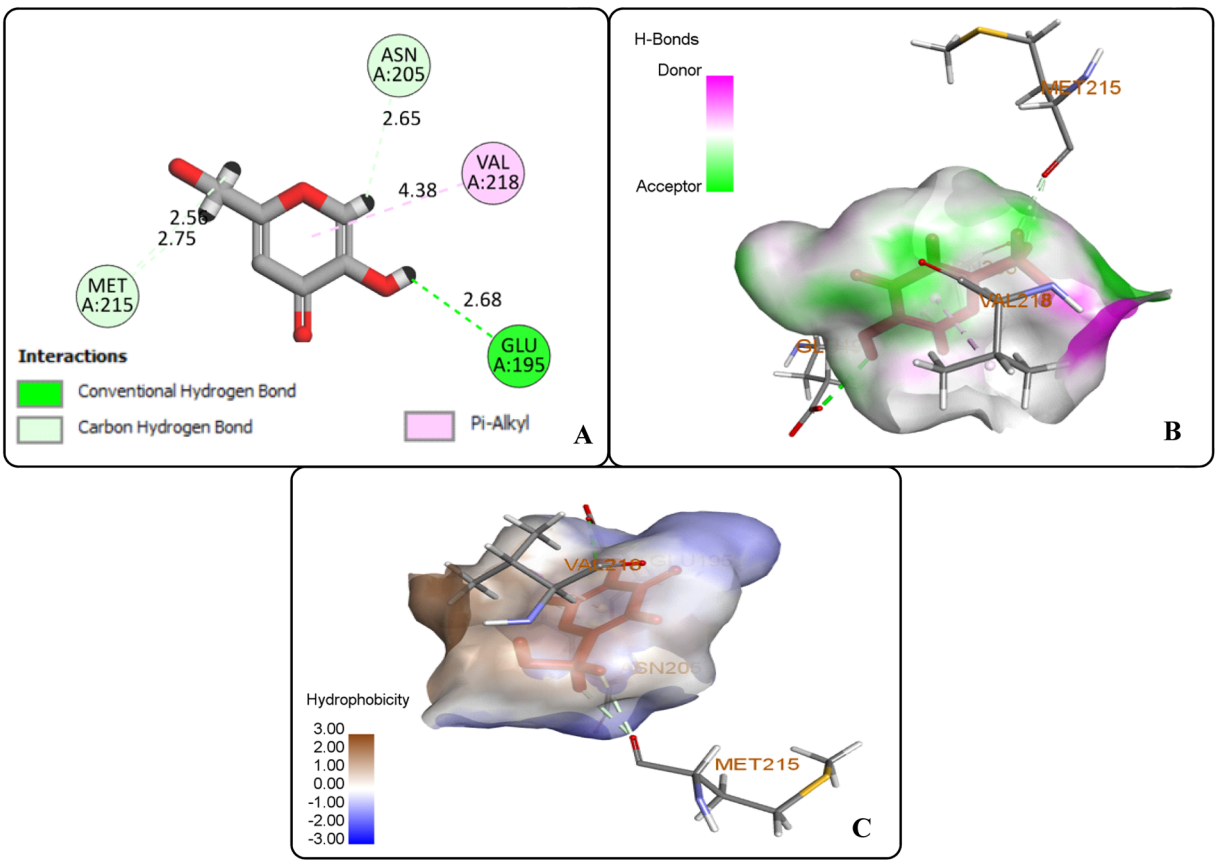

Fig. 7 Protein–ligand interactions of kojic acid: (A) 2D interactions, (B) hydrogen bonding interactions, and (C) hydrophobic interactions.

ring was found to develop hydrophobic interactions with PRO-201 (π–alkyl) *via* 4.71 Å bond distance and π–π T-shaped interactions with PHE-197 at a bond distance of 4.72 Å. Similarly, naphthofuran rings underwent hydrophobic interactions with ALA-221 (π–alkyl) *via* 4.64 Å and HIS-204 (π–π T-shaped) *via* 5.57 Å and 5.42 Å bond distances. Moreover, phenyl ring attached to triazole moiety and naphthofuran ring were found to engage in hydrophobic interactions (π–alkyl and π–σ interactions, respectively) with VAL-218 residue *via* a bond distance of 5.17 Å and 2.86 Å, respectively. In addition, the sulphur atom of compound **20i** formed π–sulfur linkage with PHE-197 at 5.97 Å bond distance (Fig. 8(A–C)).

The docking studies of **20f** revealed that the oxygen atom of the carbonyl functionality and furan ring exhibited carbon–hydrogen bonding interactions with PRO-201 and ARG-209 at 2.61 Å and 2.82 Å, respectively. The benzene ring of the anilide fragment formed a π–sulfur hydrophobic interactions with MET-184 that was 4.97 Å in the bond distance. Similarly, triazole ring was observed to be involved in π–alkyl hydrophobic interactions with PRO-201 and ARG-209 at a distance of 4.87 Å and 5.38 Å, respectively. Moreover, the furan ring showed π–alkyl hydrophobic interactions with ARG-209 and VAL-218 *via* 5.40 Å and 5.14 Å bond distances, respectively. Furthermore, the π–alkyl hydrophobic interactions were found to establish between fused benzene rings of naphthofuran functionality and amino acid residues *i.e.*, VAL-218 (*via* 4.36 Å and 4.75 Å) and ALA-221 (*via* 5.27 Å). In addition, benzene ring attached to the triazole scaffold also formed π–alkyl hydrophobic interactions with VAL-218 at 2.82 Å bond distance. Thus, induced fit docking results supported the experimental findings that identified compound **20f** and **20i** as potent tyrosinase inhibitors (Fig. 9(A–C)).

2.4. Kinetic studies

The most potent derivative **20f** was subjected to kinetic studies against diverse concentrations of tyrosine substrate (0.1–1 mM) to find out the inhibition mode and inhibition constants. The ES (K_i) and ESI (K_i') constants were determined to assess the inhibition potency of synthesized hybrid **20f** against free enzyme and ES-complex (enzyme–substrate complex). To determine the type of inhibition, Lineweaver–Burk plot was plotted ($1/V$ *versus* $1/[S]$), which indicated that the compound **20f** inhibited the activity of tyrosinase enzyme non-competitively. As the value of V_{max} was observed to change without influencing the K_m value, which was interpreted to be 0.06. The value of K_i (EI dissociation constant) and K_i' (ESI dissociation constant) for the derivative **20f** were inferred to be

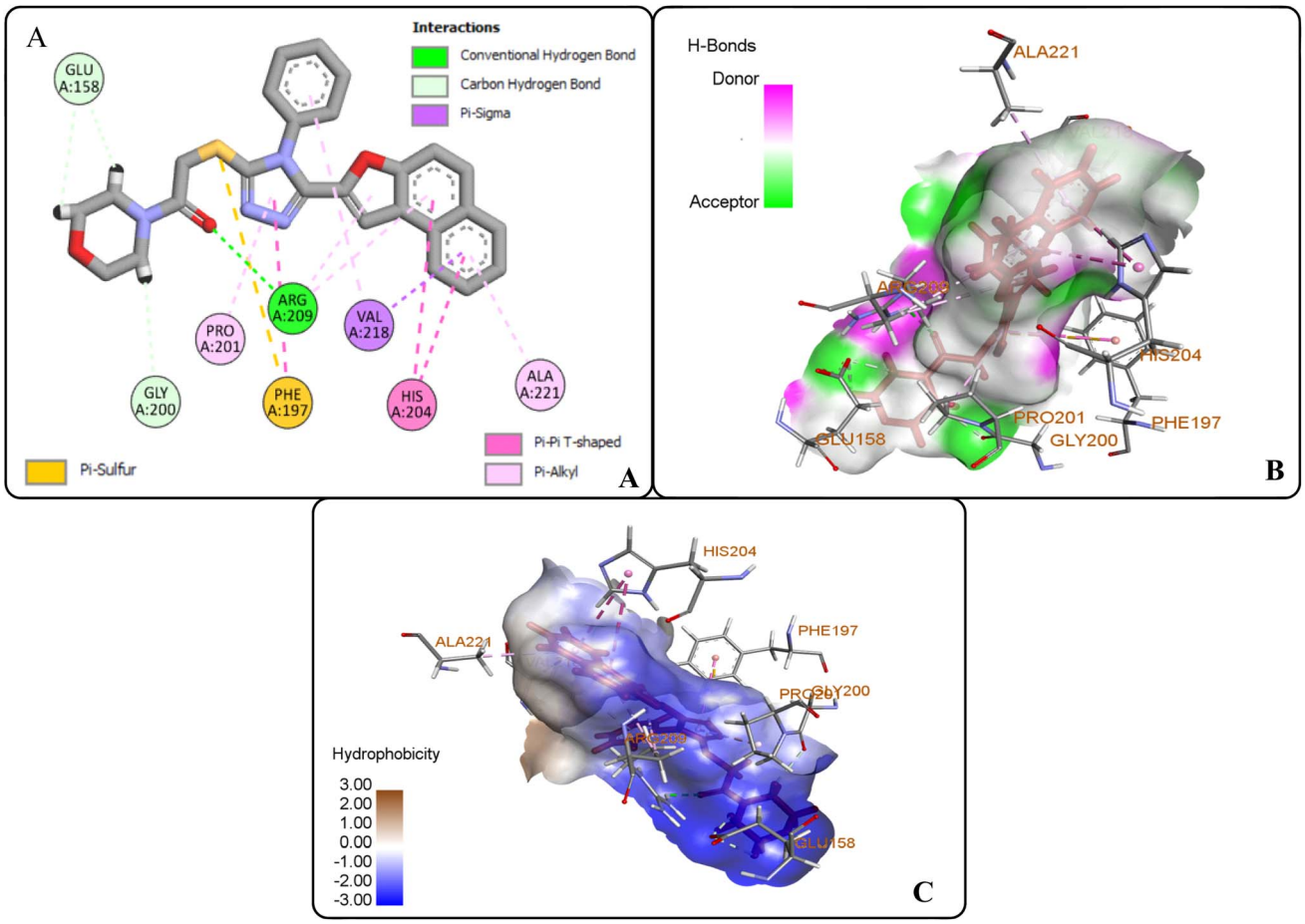

Fig. 8 Protein–ligand interactions of **20i**: (A) 2D interactions, (B) hydrogen bonding interactions, and (C) hydrophobic interactions.

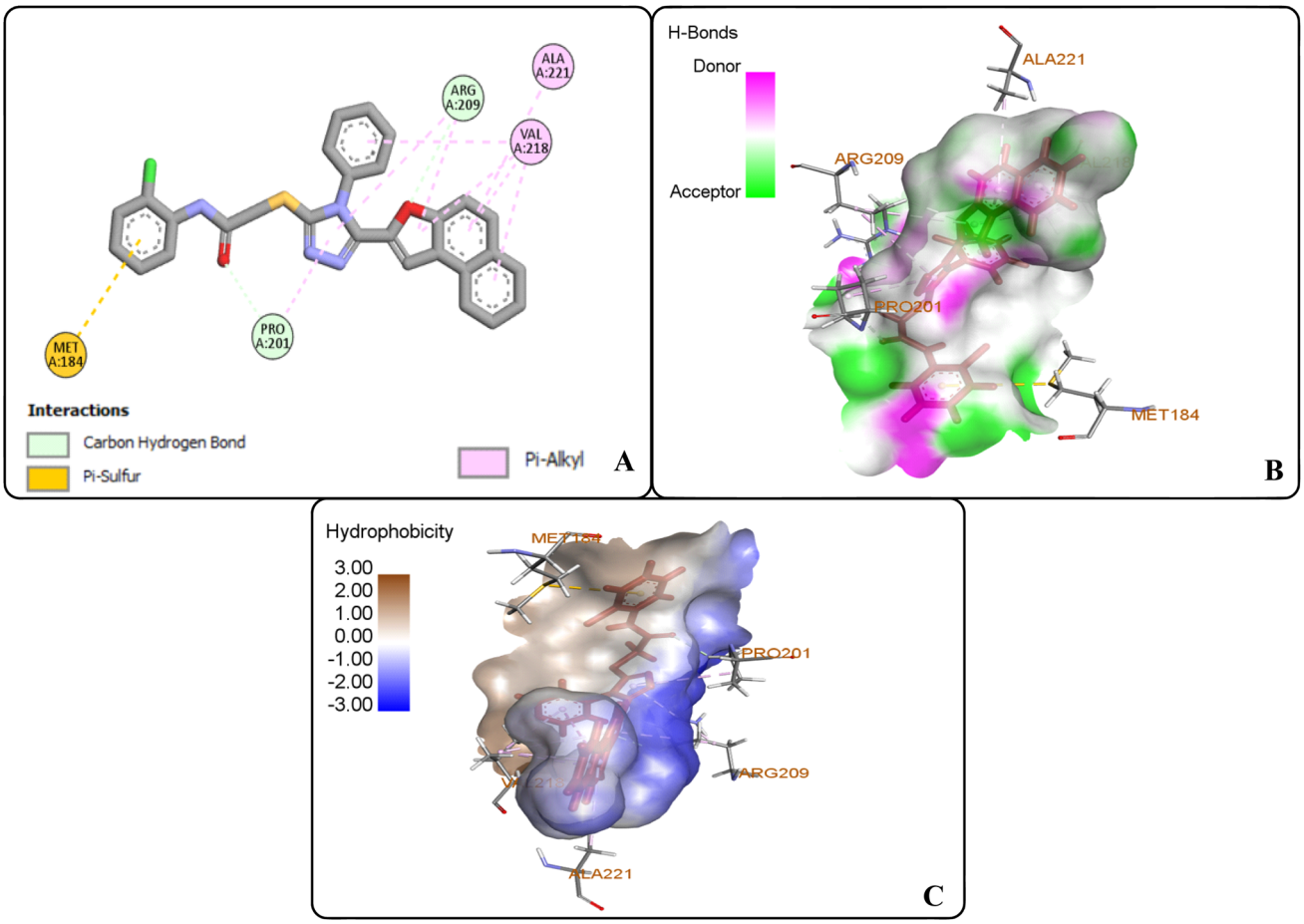

Fig. 9 Protein–ligand interactions of **20f**: (A) 2D interactions, (B) hydrogen bonding interactions, and (C) hydrophobic interactions.

0.07 and 1.77 mM, respectively, as calculated from both curves of the Lineweaver–Burk plot (Fig. 10). In addition, the Dixon plot was also sketched by plotting inhibitor concentrations against inverse of velocities, which further verified the non-competitive type enzyme inhibition activity (Fig. 11).

2.5. Structure–activity relationship

On the basis of the *in vitro* tyrosinase assay and computational studies inferences, structure–activity relationship of the synthesized naphthofuran-triazole conjugates was deduced. The enzyme inhibitory potential of different synthesized compounds was found to be dependent upon the type of

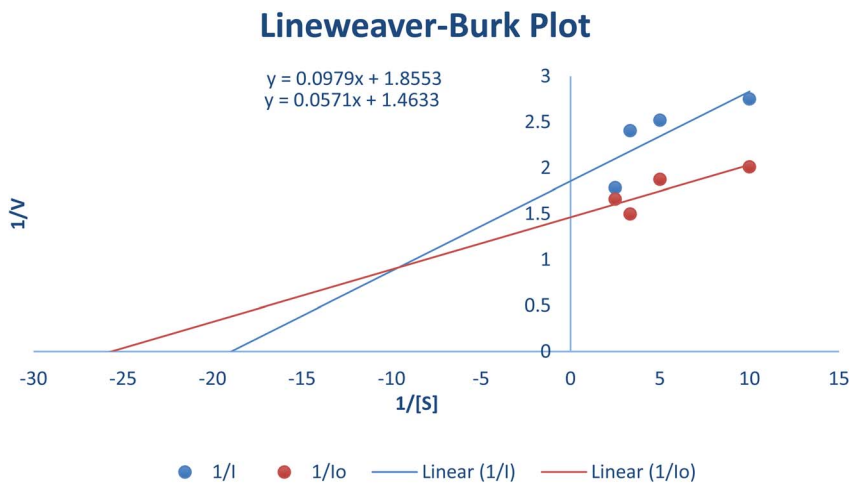

Fig. 10 Lineweaver–Burk Plot depicting the enzyme inhibition activity of tyrosinase enzyme in the presence of the potent hybrid **20f**.

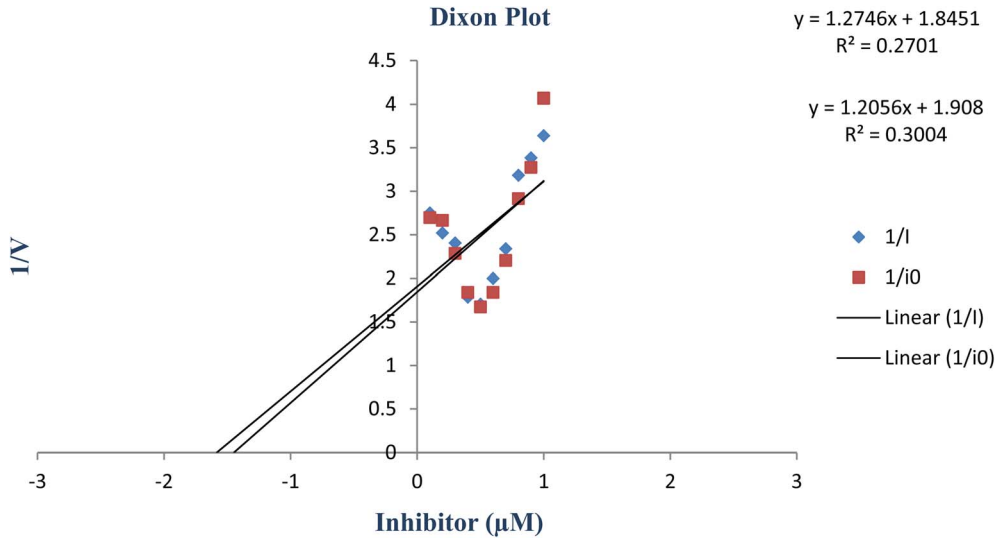

Fig. 11 Dixon plot of the concentrations of derivative **20f** (inhibitor) *vs.* the reciprocal of the enzyme velocities.

substituted Ar group. It was observed from the structure–activity relationship (SAR) that compound **20f** employing Ar as 2-ClPh exhibited the most potent enzyme inhibition activity along with the most efficient binding score of −7.10 kcal mol^{-1} owing to the presence of the electronegative group, *i.e.*, Cl on the ortho position of the phenyl ring. Similarly, by substituting Ar = morpholine, **20i**, was synthesized, which also manifested efficient IC_{50} = 1.99 μM and docking score of −6.95, thereby acting as the second-most potent enzyme inhibitory agent in comparison to standard kojic acid (displaying IC_{50} value of 30.34 with −5.03 docking score) (Fig. 12).

However, it was observed from the obtained results that the derivatives obtained by substituting electron-donating groups bearing phenyl rings (**20a**, **20b**, **20c**, **20d** & **20e**) showed comparatively low potency with IC_{50} ranging between 3.37 and 5.29. Among these five hybrids, 2,5-dimethyl substituted phenyl ring endowed hybrid **20b** exhibited efficient bacterial tyrosinase inhibition with an IC_{50} value of 3.37 ± 0.13 μM. Moreover, substitution of the methyl and *n*-butyl group at the para position on the phenyl ring of synthesized hybrids **20d** and **20a** resulted in promising IC_{50} values of 4.46 ± 0.25 μM and 4.88 ± 0.17 μM respectively. Moreover, electron-donating effect of 2,5-dimethoxy substituted phenyl ring on derivative **20d** and ethyl linked naphthofuran-triazole conjugate **20c** contributed to the relative lowering of bacterial tyrosinase inhibition potential, as indicated by their respective IC_{50} values (5.63 ± 0.12 μM and 5.29 ± 0.15 μM) (Fig. 13).

However, the 4-flouro phenyl ring-substituted naphthofuran derivative (**20h**) portrayed less inhibition activity (with IC_{50} = 9.63 μM), as compared to **20f**, bearing an electronegative group at the ortho position. Overall, among the synthesized derivatives, **20g** & **20j** (with 2-methoxy substitution at the phenyl ring group and diethyl substitution, respectively) were found to be least potent with IC_{50} values of 12.9 & 23.03 μM, respectively, among the other synthesized hybrids. Thus, the SAR interpretation inferred that the presence of electron donating groups substituted Ar functionality on prepared naphthofuran-triazole conjugates is the main factor behind the low enzyme inhibition activity. The bacterial tyrosinase inhibition potential of synthesized hybrids and reference standards is in the following order: **20f** > **20i** > **20b** > **20e** > **20a** > **20c** > **20d** > **20h** > ascorbic acid > **20g** > **20j** > kojic acid.

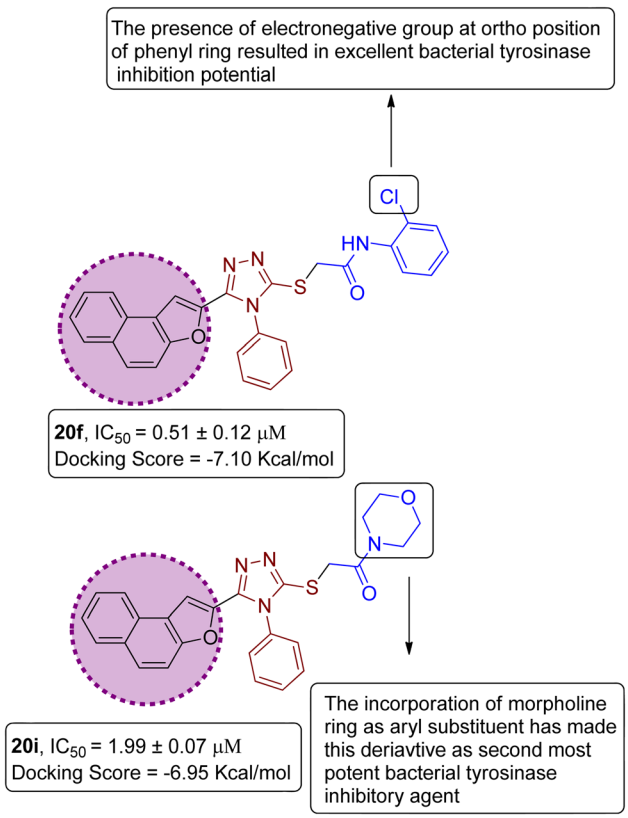

Fig. 12 Structure–activity relationship of most efficient bacterial tyrosinase inhibitors **20f** & **20i**.

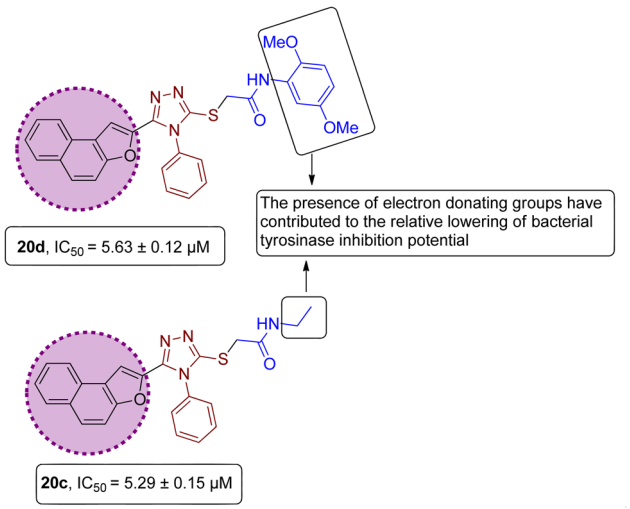

Fig. 13 Structure–activity relationship of bacterial tyrosinase inhibitors 20d & 20c.

2.6. ADMET analysis

The ADMET properties are determined as a preliminary step towards the process of drug development and its discovery. All of the synthesized naphthofuran-triazole conjugates **20(a–j)** were subjected to ADMET evaluation by processing compounds *via* online software ADMETlab 3.0. ADMETlab 3.0 is an updated software which offers detailed insights regarding ADMET features involving physiochemical, absorption, distribution, medicinal chemistry parameters, metabolism, excretion and toxicity values. Significant ADMET properties of all synthesized hybrids were focused to provide assistance in drug design process which include molecular weight, no. of rotatable bonds no. of hydrogen bond donors (*n*HD) and acceptors (*n*HA), log *P*, total polar surface area (TPSA) log, Lipinski's rule of five validation and synthetic accessibility score. Moreover, Caco-2-permeablity, human intestinal absorption, MDCK permeability scores, Pgp-inhibitor & substrate probability with blood–brain barrier probability scores. In addition, several metabolism, excretion and toxicity features of synthesized hybrids were also estimated.

Lipinski's rule of five states that a molecule must possess certain physiochemical features to behave like a drug candidate which include (a) HBD; equal or less than 5 (b) HBA: equal or less than 10 (c) MW; equal or less than 500 Da (d) log *P*; equal or less than 5. The interpretation of physiochemical properties of synthesized hybrids revealed their compatibility with the Lipinski's rule of five except **20a**, due to exceeding molecular weight than 500 along with log *P* value greater than 5. However, for hybrids **20(b–j)**, Lipinski's rule was accepted. Lipinski's rule is considered rejected for a compound, if it violates more than one mentioned physiochemical parameters. Synthetic accessibility score (Synth) was determined to be efficient for all prepared derivatives (Table 4).

Caco-2-permeability refers to the intestinal permeability, which is estimated to predict the *in vivo* absorption of the drug candidate. Any value higher than −5.15 log unit corresponds to optimal permeability. All of the prepared derivatives depicted excellent permeability, along with remarkable human intestinal

Table 4 Physiochemical and medicinal properties of synthesized hybrids 20(a–j)

Compound	Molecular weight	*n*HA	*n*HD	Log *P*	TPSA log	*n*Rot	Synthetic accessibility score	Lipinski's rule
20a	532.19	6	1	6.275	72.95	10.0	2.0	Rejected
20b	504.16	6	1	4.573	72.95	7.0	2.0	Accepted
20c	428.13	6	1	3.384	72.95	7.0	2.0	Accepted
20d	536.15	8	1	4.386	91.41	9.0	2.0	Accepted
20e	490.15	6	1	4.599	72.95	7.0	2.0	Accepted
20f	510.09	6	1	4.552	72.95	7.0	2.0	Accepted
20g	506.14	7	1	4.256	82.18	8.0	2.0	Accepted
20h	494.12	6	1	4.412	72.95	7.0	2.0	Accepted
20i	470.14	7	0	2.688	73.39	6.0	2.0	Accepted
20j	456.16	6	0	3.805	64.16	8.0	2.0	Accepted

Table 5 Absorption and distribution properties of synthesized hybrids 20(a–j)

Compound	Caco-2 permeability	HIA	BBB	PPB	MDCK-permeability	Pgp-inhibitor	Pgp-substrate	VDss
20a	−4.972	0.015	0.512	99.367	−4.614	0.971	0.0	0.629
20b	−5.031	0.0	0.884	97.656	−4.63	0.992	0.0	0.374
20c	−5.111	0.003	0.386	96.617	−4.691	0.324	0.188	−0.378
20d	−4.93	0.02	0.2	98.131	−4.542	0.943	0.0	0.325
20e	−5.077	0.001	0.767	97.504	−4.63	0.97	0.0	0.319
20f	−5.074	0.0	0.87	97.45	−4.696	0.868	0.0	0.368
20g	−5.027	0.002	0.716	97.504	−4.62	0.949	0.0	0.196
20h	−5.038	0.001	0.943	97.361	−4.567	0.984	0.0	0.267
20i	−5.065	0.002	0.346	93.793	−4.659	0.446	0.0	2.858
20j	−4.777	0.0	0.983	94.552	−4.668	0.476	0.039	−0.241

Table 6 Metabolism and excretion features of synthesized hybrids 20(a–j)

Compound	CYP1A2 inhibitor	CYP2C19 inhibitor	CYP2C9 inhibitor	CYP2D6 inhibitor	CYP3A4 inhibitor	CYP2B6 inhibitor	CYP2C8 inhibitor	CL_{Plasma}
20a	0.705	0.999	0.998	0.999	0.41	0.677	1.0	2.202
20b	0.092	1.0	0.997	0.986	0.991	0.785	1.0	1.826
20c	0.199	0.029	0.001	0.0	0.993	0.005	0.971	2.909
20d	0.971	1.0	0.344	0.999	1.0	0.758	1.0	1.897
20e	0.022	0.987	0.998	0.993	0.963	0.789	1.0	1.822
20f	0.9	1.0	0.998	0.999	0.999	0.364	1.0	2.049
20g	0.055	1.0	0.805	1.0	1.0	0.902	1.0	2.063
20h	0.034	0.988	0.995	1.0	0.621	0.277	1.0	1.648
20i	0.003	0.011	0.0	0.0	0.947	0.0	0.841	2.858
20j	0.187	0.009	0.001	0.0	0.829	0.003	0.976	3.885

Table 7 Toxicity estimation of the prepared derivatives of synthesized hybrids 20(a–j)

Compound	Eye corrosion	Carcinogenicity	Respiratory toxicity	AMES toxicity	Eye irritation
20a	0.0	0.264	0.558	0.373	0.319
20b	0.0	0.625	0.323	0.665	0.152
20c	0.0	0.816	0.384	0.677	0.248
20d	0.0	0.6999	0.383	0.725	0.066
20e	0.0	0.481	0.453	0.66	0.343
20f	0.0	0.569	0.415	0.58	0.124
20g	0.0	0.574	0.309	0.664	0.133
20h	0.0	0.589	0.391	0.731	0.241
20i	0.0	0.889	0.396	0.611	0.278
20j	0.0	0.724	0.664	0.443	0.176

absorption values. More specifically, hybrids **20b**, **20f** and **20j** exhibited efficient HIA absorption output values. In addition, all of the prepared hybrids depicted efficient volume distribution (VDss) except **20c** and **20j**. Compound with optimal value of blood–brain barrier (BBB) refers to its efficient lipophilicity and the output values of synthesized hybrids for BBB indicate their probability to act as blood-brain permeable drug like candidates. The output values for Pgp-substrate and Pgp-inhibitor correlates to their tendency to behave as corresponding substrate and inhibitor (Table 5).

The metabolism properties indicate the probability of the prepared hybrids to act as CYP-based 1A2, 2C19, 2C9, 2D6, 3A4, 2B6 and 2C8 inhibitors. The results inferred that **20c**, **20i** & **20j** has about less tendency to act as inhibitors, which certainly decrease the possibility of drug–drug interactions. In addition, CL_{plasma} values were also determined to estimate the excretion or clearance of drug-like candidates from the plasma. The CL_{plasma} values of all of the synthesized hybrids were determined to be less than 5 mL min^{-1} kg^{-1}, indicating increased efficacy and improved bioavailability (Table 6).

The synthesized hybrids were also assessed for their possible toxic effects as eye corrosive, eye irritant and carcinogenic agents. Their potential respiratory and AMES toxicity probabilities were also determined. The output values indicate their probability of being toxic or non-toxic. The ADMET results inferred the non-corrosive and non-irritant nature of all synthesized hybrids **20(a–j)**. Moreover, all hybrids depicted the low probability of being respiratory toxic. In addition, most of the synthesized derivatives were determined to be non-carcinogenic and non-AMES toxic. The results clearly illustrate the non-toxic and non-carcinogenic nature of the most potent tyrosinase inhibitor *i.e.*, **20f** (Table 7).

3. Conclusion

Here, we have synthesized a series of novel naphthofuran-based derivatives, which were then assessed for their tyrosinase inhibition activity. All the newly developed naphthofuran-incorporated derivatives were determined to be potent tyrosinase inhibitors. Among them, **20f** & **20i** were revealed to be promising tyrosinase inhibitors with $IC_{50} = 0.51 \pm 0.12$ μM & 1.99 ± 0.07 μM in comparison to both standard tyrosinase inhibitors *i.e.*, kojic and ascorbic acid. The chloro-substituted (at the ortho position) naphthofuran derivative **20f** was found to be the most efficient tyrosinase inhibitor, among all the evaluated samples and standards. The tyrosinase inhibition results were found to be in accordance with molecular docking analysis, as **20f** depicted the lowest docking score −7.10 kcal mol^{-1}. The derivative **20f** was observed to inhibit tyrosinase activity by forming carbon–hydrogen bonding, π–alkyl hydrophobic interactions and π–sulfur interactions within the active site of tyrosinase enzyme. Thus, the *in vitro* and computational studies revealed the biological potential of **20f** as a potential lead compound for the development of novel and

efficacious anti-tyrosinase drug. These findings will certainly assist scientists in carefully analyzing the pharmacological features of drug-like candidates in the drug design process (as approved by Lipinski's rule of five).

4. Experimental

4.1. Chemicals and instruments

All the solvents, reagents and precursors were obtained in analytical grade from Alfa Aesar (Ward Hill, MA, USA), Merck (Burlington, MA, USA), and Sigma-Aldrich (St. Louis, MO, USA). The purchased chemicals were employed in their original form without carrying out any additional purification technique. The progress of reactions was monitored by using thin layer chromatography, employing *n*-hexane and ethylacetate ratio as developing solvent. The melting points of synthesized compounds were obtained by utilizing WRS-1B mp apparatus. ^{1}H-NMR and ^{13}C-NMR spectroscopy was carried out by utilizing Bruker 400 MHz FT-NMR spectrophotometer, TMS (tetramethylsilane) as an internal standard in $CDCl_3$. The obtained spectra were then analyzed by using MestReNova. The values of coupling constant were represented in hertz. The multiplicity of peaks were presented by symbols 's' (singlet), 'd (doublet)' 'dd (doublet of doublet)' & 'm (multiplet)'. The newly prepared naphthofuran derivatives were purified by using column chromatography.

4.2. General synthetic protocol

To a mixture of 5-(naphtho[2,1-*b*]furan-2-yl)-4-phenyl-4*H*-1,2,4-triazole-3-thiol **17** (65 mg, 0.18 mmol) in dimethylformamide (5 mL), potassium carbonate (29 mg, 0.2 mmol), KI (5.3 mg, 0.03 mmol) and CTAB (3.2 mg, 0.009 mmol) were added. Then, the diversely substituted bromoacetanilides **19** (0.19 mmol) were introduced to the reaction mixture, which was sonicated at 80 °C for about 20 min to one an hour. The completion of the reaction was verified by carrying out thin layer chromatography. After confirmation of completion of the reaction, ice-cold distilled water was added to the reaction mixture. The resulting precipitates were then filtered and purified by column chromatography.

4.2.1. *N*-(4-butylphenyl)-2-((5-(naphtho[2,1-*b*]furan-2-yl)-4-phenyl-4*H*-1,2,4-triazol-3-yl)thio)acetamide 20a. Off-white powder; 84%; R_f: 0.45 (*n*-hexane/ethylacetate 1 : 1); mp 220–225 °C ^{1}H-NMR (400 MHz, $CDCl_3$): δ 0.88 (t, J = 8 Hz, 3H), 1.26–1.35 (m, 2H), 1.54 (q, J = 8 Hz, 2H), 2.54 (t, J = 8 Hz, 2H), 4.03 (s, 2H), 6.97 (s, 1H), 7.10 (d, J = 8 Hz, 2H), 7.42–7.49 (m, 3H), 7.51–7.57 (m, 4H), 7.62–7.75 (m, 4H), 7.875 (dd, J = 8 Hz, 2H), 10.23 (s, 1H); ^{13}C-NMR ($CDCl_3$, 100 MHz): 13.9, 22.2, 33.6, 35.0, 36.2, 107.0, 112.2, 119.6, 119.7, 122.8, 123.0, 125.2, 126.9, 127.3, 127.4, 127.6, 128.7, 128.7, 128.7, 128.9, 130.4, 130.4, 130.4, 131.1, 132.8, 135.8, 138.9, 141.4, 148.3, 152.9, 154.2, 166.0; LC-MS(ESI) (*m*/*z*) calculated for $C_{32}H_{28}N_4O_2S$ is 532.1; found: 532.9 [M^+].

4.2.2. *N*-(2,5-dimethylphenyl)-2-((5-(naphtho[2,1-*b*]furan-2-yl)-4-phenyl-4*H*-1,2,4-triazol-3-yl)thio)acetamide 20b. White coarse solid; 74%, R_f: 0.79 (*n*-hexane/ethylacetate 1 : 1); mp 236–240 °C. ^{1}H-NMR (400 MHz, $CDCl_3$): δ 2.29 (s, 3H), 2.36 (s, 3H), 4.15 (s, 2H), 6.85 (d, J = 8 Hz, 1H), 7.05 (d, J = 8 Hz, 1H), 7.08 (s, 1H), 7.43–7.56 (m, 5H), 7.62–7.78 (m, 5H), 7.88 (t, J = 8 Hz, 2H), 9.64 (s, 1H); ^{13}C-NMR ($CDCl_3$, 100 MHz): 18.0, 21.1, 36.0, 107.5, 112.2, 122.7, 123.0, 123.1, 125.2, 125.7, 126.3, 126.9, 127.3, 127.3, 127.3, 127.7, 128.8, 130.2, 130.4, 130.4, 130.4, 131.2, 132.7, 135.8, 136.1, 141.1, 148.2, 153.0, 154.1, 166.3; LC-MS(ESI) (*m*/*z*) calculated for $C_{30}H_{25}N_4O_2S$ is 505.1; found: 505.2 [M^+ + H].

4.2.3. *N*-ethyl-2-((5-(naphtho[2,1-*b*]furan-2-yl)-4-phenyl-4*H*-1,2,4-triazol-3-yl)thio)acetamide 20c. Off-white solid; 84%; R_f: 0.19 (*n*-hexane/ethylacetate 1 : 1); mp 206–208 °C. ^{1}H-NMR (400 MHz, $CDCl_3$): δ 1.15 (t, J = 8 Hz, 3H), 3.26–3.33 (m, 2H), 3.84 (s, 2H), 6.94 (s, 1H), 7.40 (d, J = 8 Hz, 2H), 7.47 (d, J = 8 Hz, 1H), 7.53 (d, J = 8 Hz, 2H), 7.60–7.67 (m, 4H), 7.725 (d, J = 12 Hz, 1H), 7.85–7.90 (m, 2H); ^{13}C-NMR ($CDCl_3$, 100 MHz); δ 14.5, 34.8, 35.1, 106.6, 112.2, 112.8, 123.1, 125.1, 126.8, 125.5, 130.3, 130.4, 131.0, 133.0, 141.8, 148.4, 152.8, 153.7, 168.1; LC-MS(ESI) (*m*/*z*) calculated for $C_{24}H_{21}N_4O_2S$ is 429.1; found: 429.0 [M^+ + H].

4.2.4. *N*-(2,5-dimethoxyphenyl)-2-((5-(naphtho[2,1-*b*]furan-2-yl)-4-phenyl-4*H*-1,2,4-triazol-3-yl)thio)acetamide 20d. Brown coarse solid; 92%; R_f: 0.28 (*n*-hexane/ethylacetate 1 : 1) mp 188–191 °C. ^{1}H-NMR (400 MHz, $CDCl_3$): δ 3.74 (s, 3H), 3.90 (s, 3H), 4.15 (s, 2H), 6.56 (s, 1H), 6.76 (d, J = 8 Hz, 1H), 7.15 (s, 1H), 7.43–7.73 (m, 9H), 7.89 (s, 2H), 8.04 (s, 1H), 9.65 (s, 1H); ^{13}C-NMR ($CDCl_3$, 100 MHz): 36.3, 55.7, 56.6, 106.3, 107.4, 109.0, 111.1, 112.2, 122.8, 123.2, 125.2, 126.9, 127.3, 127.3, 127.3, 127.5, 128.4, 128.8, 130.2, 130.2, 130.4, 131.0, 132.9, 141.4, 142.9, 148.1, 152.9, 153.3, 153.6, 166.0; LC-MS(ESI) (*m*/*z*) calculated for $C_{30}H_{24}N_4O_4S$ is 536.1; found: 536.9 [M^+].

4.2.5. 2-((5-(Naphtho[2,1-*b*]furan-2-yl)-4-phenyl-4*H*-1,2,4-triazol-3-yl)thio)-*N*-(*p*-tolyl)acetamide 20e. Light brown solid; 88%; R_f: 0.45 (*n*-hexane/ethylacetate 1 : 1); mp 210–214 °C. ^{1}H-NMR (400 MHz, $CDCl_3$): δ 2.28 (s, 3H), 4.01 (s, 2H), 6.95 (s, 1H), 7.10 (d, J = 8 Hz, 2H), 7.41–7.49 (m, 3H), 7.54 (d, J = 8 Hz, 3H), 7.61–7.70 (m, 4H), 7.74 (d, J = 8 Hz, 1H), 7.88 (q, J = 8 Hz, 2H), 10.23 (s, 1H); ^{13}C-NMR ($CDCl_3$, 100 MHz): 20.8, 36.2, 106.8, 112.2, 119.6, 119.7, 122.81, 123.0, 125.2, 126.8, 127.3, 127.4, 127.6, 128.9, 129.3, 129.3, 130.4, 130.4, 130.4, 130.4, 131.1, 132.9, 133.8, 135.6, 141.5, 148.3, 152.9, 154.2, 166.1; LC-MS(ESI) (*m*/*z*) calculated for $C_{29}H_{22}N_4O_2S$ is 490.1; found: 490.9 [M^+].

4.2.6. *N*-(2-chlorophenyl)-2-((5-(naphtho[2,1-*b*]furan-2-yl)-4-phenyl-4*H*-1,2,4-triazol-3-yl)thio)acetamide 20f. Off-white solid; 76%; R_f: 0.44 (*n*-hexane/ethylacetate 1 : 1); mp 232–236 °C. 1H-NMR (400 MHz, $CDCl_3$): δ 4.19 (s, 2H), 7.03 (t, J = 8 Hz, 1H), 7.18 (s, 1H), 7.36 (d, J = 8 Hz, 1H), 7.44 (d, J = 8 Hz, 2H), 7.48 (d, J = 8 Hz, 1H), 7.53 (dd, J = 8 Hz, 2H), 7.61–7.68 (m, 4H), 7.73 (d, J = 8 Hz, 1H), 7.90 (t, J = 8 Hz, 2H), 8.28 (d, J = 8 Hz, 1H), 9.84 (s, 1H); ^{13}C-NMR ($CDCl_3$, 100 MHz): 36.0, 100.7, 112.2, 122.4, 122.8, 122.8, 123.1, 125.1, 125.2, 126.9, 127.3, 127.3, 127.3, 128.8, 128.8, 128.7, 129.3, 129.3, 130.3, 130.3, 130.3, 130.4, 131.1, 144.6, 145.4, 148.1, 153.0, 166.6; LC-MS(ESI) (*m*/*z*) calculated for $C_{28}H_{20}ClN_4O_2S$ is 511.0; found: 511.1 [M^+ + H].

4.2.7. *N*-(2-methoxyphenyl)-2-((5-(naphtho[2,1-*b*]furan-2-yl)-4-phenyl-4*H*-1,2,4-triazol-3-yl)thio)acetamide 20g. Off-white powder: 79%, R_f: 0.41(*n*-hexane/ethylacetate 1 : 1); mp 197–199 °C. ^{1}H-NMR (400 MHz, $CDCl_3$): δ 3.95 (s, 3H), 4.16 (s, 2H),

6.85 (d, $J = 8$ Hz, 1H), 6.92 (t, $J = 8$ Hz, 1H), 7.03 (t, $J = 8$ Hz, 1H), 7.16 (s, 1H), 7.43–7.56 (m, 5H), 7.62–7.74 (m, 4H), 7.90 (d, $J =$ 8 Hz, 2H), 8.30 (d, $J = 8$ Hz, 1H), 9.65 (s, 1H); ^{13}C-NMR ($CDCl_3$, 100 MHz): 36.5, 56.0, 107.4, 110.2, 112.2, 120.1, 120.7, 122.8, 123.2, 124.1, 125.2, 126.9, 127.3, 127.5, 127.5, 127.5, 127.7, 128.8, 128.8, 130.3, 130.3, 130.3, 130.4, 131.0, 132.9, 141.5, 148.7, 152.9, 166.0; LC-MS(ESI) (m/z) calculated for $C_{29}H_{22}N_4O_3S$ is 506.1; found: 506.9 [M^+].

4.2.8. *N*-(4-fluorophenyl)-2-((5-(naphtho[2,1-*b*]furan-2-yl)-4-phenyl-4*H*-1,2,4-triazol-3-yl)thio)acetamide 20h. Tan/light brown solid; 80%, R_f: 0.57 (*n*-hexane/ethylacetate 1 : 1); mp 229–232 °C. ^{1}H-NMR (400 MHz, $CDCl_3$): δ 4.15 (s, 2H), 6.97 (t, J = 8 Hz, 2H), 7.07 (s, 1H), 7.46–7.56 (m, 5H), 7.6525 (dd, $J = 4$ Hz, 4H), 7.7275 (dd, $J = 12$ Hz, 2H), 7.88 (t, $J = 8$ Hz, 2H), 10.54 (s, 1H); ^{13}C-NMR ($CDCl_3$, 100 MHz): 36.4, 108.1, 112.1, 115.3, 115.5, 121.4, 122.7, 123.0, 125.3, 127.0, 127.3, 127.3, 127.3, 128.1, 128.9, 128.9, 130.4, 130.5, 130.5, 130.5, 131.4, 132.4, 134.2, 141.6, 147.4, 152.1, 153.1, 165.7; LC-MS(ESI) (m/z) calculated for $C_{28}H_{19}FN_4O_2S$ is 494.1; found: 494.9 [M^+].

4.2.9. 1-Morpholino-2-((5-(naphtho[2,1-*b*]furan-2-yl)-4-phenyl-4*H*-1,2,4-triazol-3-yl)thio)ethanone 20i. Lemon yellow solid; 77%; R_f: 0.09 (*n*-hexane/ethylacetate 1 : 1); mp 140–143 °C. ^{1}H-NMR (400 MHz, $CDCl_3$): δ 3.61–3.75 (m, 8H), 4.47 (s, 2H), 7.12 (s, $J = 8$ Hz, 1H), 7.44–7.56 (m, 5H), 7.61–7.68 (m, 3H), 7.725 (d, $J = 12$ Hz, 1H), 7.89 (d, $J = 8$ Hz, 2H); ^{13}C-NMR ($CDCl_3$, 100 MHz): 42.5, 46.6, 46.6 66.6, 66.6, 107.5, 112.2, 112.8, 123.1, 125.2, 126.9, 127.3, 127.5, 127.5, 127.6, 128.8, 130.3, 130.3, 130.3, 130.4, 131.1, 132.8, 141.2, 147.7, 153.0, 165.3; LC-MS(ESI) (m/z) calculated for $C_{26}H_{23}N_4O_3S$ is 471.1; found: 471.2 [$M^+ + H$].

4.2.10. *N*,*N*-diethyl-2-((5-(naphtho[2,1-*b*]furan-2-yl)-4-phenyl-4*H*-1,2,4-triazol-3-yl)thio)acetamide 20j. Brown solid; 80%; R_f: 0.16 (*n*-hexane/ethylacetate 1 : 1); mp 130–132 °C. ^{1}H-NMR (400 MHz, $CDCl_3$): δ 1.12 (t, $J = 8$ Hz, 3H), 1.25 (t, $J =$ 8 Hz, 3H), 3.36–3.48 (m, 4H), 4.41 (s, 2H), 6.94 (s, 1H), 7.41–7.47 (m, 3H), 7.52–7.55 (m, 2H), 7.57–7.64 (m, 3H), 7.71 (d, $J = 8$ Hz, 1H), 7.87 (t, $J = 8$ Hz, 2H); ^{13}C-NMR ($CDCl_3$, 100 MHz); δ 12.8, 14.3, 37.1, 40.7, 42.6, 106.2, 112.3, 122.9, 123.1, 125.0, 126.7, 127.1, 127.4, 127.5, 127.5, 127.5, 128.8, 130.1, 130.1, 130.4, 130.6, 142.3, 148.0, 152.7, 153.4, 165.9; LC-MS(ESI) (m/z) calculated for $C_{26}H_{24}N_4O_2S$ is 456.1; found: 456.2 [M^+].

4.3. Biological evaluation

The isolation and purification of bacterial tyrosinase enzyme were carried out using previously developed protocols.[69,70] To investigate the tyrosinase inhibitory potential of synthesized naphthofuran-based derivatives, spectroscopic methodology was exploited to examine their respective IC_{50} values *via* reported methods.[71] For inhibition analysis, 2 mM L-tyrosine (765 μL), buffer solution (phosphate buffer solution of pH = 6.8, 0.05 mM), along with 35 μL of the test compound (dissolved in dimethyl sulfoxide) were placed in an incubator under favorable temperature conditions for almost 10 minutes. This step was followed by the addition of 200 μL of isolated bacterial tyrosinase enzyme. The test sample was subjected to incubation at 37 °C in comparison to the control and blank sample. After incubation, the inhibition potential of the synthesized derivatives was ascertained at 475 nm. The increased level of dopachrome was further investigated by measuring the absorbance at 475 nm wavelength, thereby determining the tyrosinase inhibition activity. The inhibition potential was illustrated by determining the percentage inhibition and IC_{50} values (obtained by extrapolation of the graph). The interpreted results were then critically compared with those of the standard inhibitors.

The percentage inhibition all synthesized derivatives was interpreted by given formula:

$$\text{Percentage inhibition} = (\text{absorbance of blank} - \text{absorbance of sample/absorbance of control blank}) \times 100$$

4.4. Kinetic studies

The kinetic studies of the most potent derivative **20f** were carried out by utilizing diverse concentrations of tyrosine substrate (0.1, 0.2, 0.3 0.4, 0.5, 0.6, 0.7, 0.8, 0.9 & 1 mM) and optimized concentration of inhibitor **20f** (100 μL). The time duration for pre-incubation and measurement was exactly similar to the one mentioned in the biological evaluation for the tyrosinase inhibition assay. The value of the maximum initial velocity was inferred by the initial linear duration of absorbance up to 5 min, upon the introduction of enzyme at the interval of fifteen seconds. The type of enzyme inhibition was investigated by Lineweaver–Burk plot, which was obtained by plotting the inverse of velocities ($1/V$) against the inverse of substrate concentrations ($1/[S]$) mM^{-1}. In addition, EI (K_i) and ESI (K_i') dissociation constant values were attained by the secondary plot of the slope and intercept *versus* the inhibitor concentration, respectively. The Dixon plot was also plotted to confirm the type of inhibition.

4.5. Molecular docking studies

The compounds (**20f** & **20i**) with lower IC_{50} values were selected for induced fit docking. All the docking analysis was performed in Molecular Operating Environment (MOE 2015).[72] The targeted compounds were prepared in ChemDraw software. The standard kojic acid (CID: 3840) structure was acquired from PubChem. The tyrosinase crystallized structure (5OAE) was downloaded from the Protein data bank (PDB),[73] and used as a receptor in the IFD docking. The protein and ligand structures were prepared by using QuickPrep tool of MOE. The default Amber10:EHT forcefield with gradient 0.1 was used to energy minimize the docking ligands. Induced Fit refinement, Triangular Matcher placement, London-dG, and GBVI/WSA scoring were all used for screening. The native ligand was subjected to cognate redocking in order to validate the docking protocol. The ligand–protein interaction analysis was performed in BIOVIA Discovery Studio 2024.

4.6. ADMET analysis

All of the novel naphthofuran-triazole conjugates were subjected to ADMET (Absorption, Distribution, Metabolism, Excretion and Toxicity) analysis by using online software ADMETLab 3.0.[74] The SMILES of compounds were generated by drawing the structures of derivatives on an online server, and the resulting smiles were run for ADMET evaluation.

Data availability

All data are included in the manuscript and ESI files.†

Conflicts of interest

The authors have no conflict of interest for this research work.

Acknowledgements

We are thankful for the Researchers supporting project number (RSPD2024R740), King Saud University, Riyadh, Saudi Arabia.

References

1 K. Tief, M. Hahne, A. Schmidt and F. Beermann, Tyrosinase, the key enzyme in melanin synthesis, is expressed in murine brain, *Eur. J. Biochem.*, 1996, **241**, 12–16.
2 C. S. Nunes, and K. Vogel, Tyrosinases—Physiology, pathophysiology, and applications, in *Enzymes in Human and Animal Nutrition*, Academic Press, 2018, pp. 403–412.
3 T. Nagatsu, A. Nakashima, H. Watanabe, S. Ito and K. Wakamatsu, Neuromelanin in Parkinson's disease: tyrosine hydroxylase and tyrosinase, *Int. J. Mol. Sci.*, 2022, **23**, 4176.
4 B. N. Marieshwari, S. Bhuvaragavan, K. Sruthi, P. Mullainadhan and S. Janarthanan, Insect phenoloxidase and its diverse roles: Melanogenesis and beyond, *J. Comp. Physiol., B*, 2023, **193**, 1–23.
5 K.-K. Song, H. Huang, P. Han, C.-L. Zhang, Y. Shi and Q.-X. Chen, Inhibitory effects of cis-and trans-isomers of 3, 5-dihydroxystilbene on the activity of mushroom tyrosinase, *Biochem. Biophys. Res. Commun.*, 2006, **342**, 1147–1151.
6 S. Passi and M. Nazzaro-Porro, Molecular basis of substrate and inhibitory specificity of tyrosinase: phenolic compounds, *Br. J. Dermatol.*, 1981, **104**, 659–665.
7 L. G. Fenoll, M. J. Penalver, J. N. Rodrıguez-López, R. Varón, F. Garcıa-Cánovas and J. Tudela, Tyrosinase kinetics: discrimination between two models to explain the oxidation mechanism of monophenol and diphenol substrates, *Int. J. Biochem. Cell Biol.*, 2004, **36**, 235–246.
8 X. Lai, H. J. Wichers, M. Soler-Lopez and B. W. Dijkstra, Structure and function of human tyrosinase and tyrosinase-related proteins, *Chem.–Eur. J.*, 2018, **24**, 47–55.
9 K. Lerch, Molecular and active site structure of tyrosinase, *Life Chem. Rep.*, 1987, **5**, 221–234.
10 M. Brenner and V. J. Hearing, The protective role of melanin against UV damage in human skin, *Photochem. Photobiol.*, 2008, **84**, 539–549.
11 G. M. Casañola-Martín, Y. Marrero-Ponce, M. T. H. Khan, A. Ather, K. M. Khan, F. Torrens and R. Rotondo, Dragon method for finding novel tyrosinase inhibitors: Biosilico identification and experimental *in vitro* assays, *Eur. J. Med. Chem.*, 2007, **42**, 1370–1381.
12 K. I. Nihei, Y. Yamagiwa, T. Kamikawa and I. Kubo, 2-Hydroxy-4-isopropylbenzaldehyde, a potent partial tyrosinase inhibitor, *Bioorg. Med. Chem.*, 2004, **14**, 681–683.
13 S. Dorga and R. Sarangal, Pigmentary disorders: an insight, *Pigment Int.*, 2014, **1**, 5–7.
14 Z. P. Zheng, K. W. Cheng, J. Chao, J. Wu and M. Wang, Tyrosinase inhibitors from paper mulberry (Broussonetia papyrifera), *Food Chem.*, 2008, **106**, 529–535.
15 M. Friedman, Food browning and its prevention: an overview, *J. Agric. Food Chem.*, 1996, **44**, 631–653.
16 R. F. Hurrell, and P. A. Finot, Nutritional consequences of the reactions between proteins and oxidized polyphenolic acids, in *Nutritional and Toxicological Aspects of Food Safety*, Springer, Boston, MA, US, 1984, pp. 423–435.
17 Y. J. Kim and H. Uyama, Tyrosinase inhibitors from natural and synthetic sources: structure, inhibition mechanism and perspective for the future, *Cell. Mol. Life Sci.*, 2005, **62**, 1707–1723.
18 J. P. Germanas, S. Wang, A. Miner, W. Hao and J. M. Ready, Discovery of small-molecule inhibitors of tyrosinase, *Bioorg. Med. Chem. Lett.*, 2007, **17**, 6871–6875.
19 N. W. Hsiao, T. S. Tseng, Y. C. Lee, W. C. Chen, H. H. Lin, Y. R. Chen, Y. T. Wang, H. J. Hsu and K. C. Tsai, Serendipitous discovery of short peptides from natural products as tyrosinase inhibitors, *J. Chem. Inf. Model.*, 2014, **54**, 3099–3111.
20 M. T. Smith, J. W. Yager, K. L. Steinmetz and D. A. Eastmond, Peroxidase – dependent metabolism of benzene's phenolic metabolites and its potential role in benzene toxicity and carcinogenicity, *Environ. Health Perspect.*, 1989, **82**, 23–29.
21 M. T. H. Khan, Novel tyrosinase inhibitors from natural resources–their computational studies, *Curr. Med. Chem.*, 2012, **19**, 2262–2272.
22 T. S. Chang, An updated review of tyrosinase inhibitors, *Int. J. Mol. Sci.*, 2009, **10**, 2440–2475.
23 A. Nesterov, J. Zhao and Q. Jia, Natural tyrosinase inhibitors for skin hyperpigmentation, *Drugs Future*, 2008, **33**, 945–954.
24 S. Parvez, M. Kang, H. S. Chung and H. Bae, Naturally occurring tyrosinase inhibitors: mechanism and applications in skin health, cosmetics and agriculture industries, *Phytother. Res.*, 2007, **21**, 805–816.
25 M. T. H. Khan, Molecular design of tyrosinase inhibitors: A critical review of promising novel inhibitors from synthetic origins, *Pure Appl. Chem.*, 2007, **79**, 2277–2295.
26 M. T. H. Khan, Heterocyclic compounds against the enzyme tyrosinase essential for melanin production: biochemical features of inhibition, *Bioact. Heterocycl.*, 2007, **III**, 119–138.
27 A. Rescigno, F. Sollai, B. Pisu, A. Rinaldi and E. Sanjust, Tyrosinase inhibition: general and applied aspects, *J. Enzyme Inhib. Med. Chem.*, 2002, **17**, 207–218.
28 L. Xia, A. Idhayadhulla, Y. R. Lee, Y.-J. Wee and S. H. Kim, Anti-tyrosinase, antioxidant, and antibacterial activities of novel 5-hydroxy-4-acetyl-2, 3-dihydronaphtho [1, 2-b] furans, *Eur. J. Med. Chem.*, 2014, **86**, 605–612.
29 V. Srivastava, A. S. Negi, J. K. Kumar, U. Faridi, B. S. Sisodia, M. P. Darokar, S. Luqman and S. P. S. Khanuja, Synthesis of

1-(3′,4′,5′-trimethoxy) phenyl naphtho [2, 1b] furan as a novel anticancer agent, *Bioorg. Med. Chem. Lett.*, 2006, **16**, 911–914.
30 W. Venegas, M. Sala, J. P. Buisson, R. Royer and I. Chouroulinkov, Relationship between the chemical structure and the mutagenic and carcinogenic potentials of five naphthofurans, *Cancer Res.*, 1984, **44**, 1969–1975.
31 C. KIRILMIŞ, M. Koca, S. Servi and S. Gür, Synthesis and antimicrobial activity of dinaphtho [2, 1-b] furan-2-yl-methanone and their oxime derivatives, *Turk. J. Chem.*, 2009, **33**, 375–384.
32 S. Nocentini, J. Coppey, J. P. Buisson and R. Royer, Inhibition of DNA synthesis in relation to enhanced survival of UV-damaged herpes virus in monkey cells treated by a variety of 2-nitronaphthofurans, *Mutat. Res., Genet. Toxicol.*, 1981, **90**, 125–135.
33 N. S. Mone, S. A. Bhagwat, D. Sharma, M. Chaskar, R. H. Patil, P. Zamboni, N. N. Nawani and S. K. Satpute, Naphthoquinones and their derivatives: emerging trends in combating microbial pathogens, *Coatings*, 2021, **11**, 434.
34 J. Gao, Q. Q. Chen, Y. Huang, K. H. Li, X. J. Geng, T. Wang, Q.-S. Lin and R. S. Yao, Design, synthesis and pharmacological evaluation of naphthofuran derivatives as potent SIRT1 activators, *Front. Pharmacol*, 2021, **12**, 653233.
35 K. M. Mahadevan, B. Padmashali and V. P. Vaidya, Studies in naphthofurans: Part V-synthesis of 2-aryl-1, 2, 3, 4-tetrahydropyrido (naphtho [2, 1-b] furan)-4-ones and their biological activity, *Indian J. Heterocycl. Chem.*, 2001, **11**, 15–20.
36 A. Idhayadhulla, L. Xia, Y. R. Lee, S. H. Kim, Y. J. Wee and C. S. Lee, Synthesis of novel and diverse mollugin analogues and their antibacterial and antioxidant activities, *Bioorg. Chem.*, 2014, **52**, 77–82.
37 R. Kenchappa and Y. D. Bodke, Synthesis, analgesic and anti-inflammatory activity of benzofuran pyrazole heterocycles, *Chem. Data Collect.*, 2020, **28**, 100453.
38 C.-Y. Hsieh, P.-C. Tsai, C.-H. Tseng, Y. Chen, L.-S. Chang and S.-R. Lin, Inhibition of EGF/EGFR activation with naphtho [1, 2-b] furan-4, 5-dione blocks migration and invasion of MDA-MB-231 cells, *Toxicol. In Vitro*, 2013, **27**, 1–10.
39 J. P. Lumb and D. Trauner, Biomimetic synthesis and structure elucidation of Rubicordifolin, a cytotoxic natural product from Rubia cordifolia, *J. Am. Chem. Soc.*, 2005, **127**, 2870–2871.
40 D. H. Miles, D. S. Lho, A. A. De la Cruz, E. D. Gomez, J. A. Weeks and J. L. Atwood, Toxicants from mangrove plant. 3. Heritol, a novel ichthyotoxin from the mangrove plant Heritiera littoralis, *J. Org. Chem.*, 1987, **52**, 2930–2932.
41 P. K. Zubaidha, S. P. Chavan, U. S. Racherla and N. R. Ayyangar, Synthesis of (±)heritol, *Tetrahedron*, 1991, **47**, 5759–5768.
42 H. Irie, R. Matsumoto, M. Nishimura and Y. Zhang, Synthesis of (±)-Heritol, a Sesquiterpene Lactone belonging to the Aromatic Cadinane Group, *Chem. Pharm. Bull.*, 1990, **38**, 1852–1856.
43 F. Bohlmann and C. Zdero, Natürlich vorkommende Terpen-Derivate, 80. Einige Inhaltsstoffe der Gattung Chromolaena, *Chem. Ber.*, 1977, **110**, 487–490.
44 K. Ishiguro, Y. Ohira and H. Oku, Antipruritic dinaphthofuran-7,12-dione derivatives from the pericarp of Impatiens balsamina, *J. Nat. Prod.*, 1998, **61**, 1126–1129.
45 A. H. F. Abdelwahab and S. A. H. Fekry, Synthesis, reactions and applications of naphthofurans: A review, *Eur. J. Chem.*, 2021, **12**, 340–359.
46 Y. Chen, Y. Tang, B. Mao, W. Li, H. Jin, L. Zhang and Z. Liu, Discovery of N-(Naphtho [1, 2-b] Furan-5-Yl) benzenesulfonamides as novel selective inhibitors of triple-negative breast cancer (TNBC), *Molecules*, 2018, **23**, 678.
47 D. K. Lang, R. Kaur, R. Arora, B. Saini and S. Arora, Nitrogen-containing heterocycles as anticancer agents: An overview, *Anti-Cancer Agents Med. Chem.*, 2020, **20**, 2150–2168.
48 A. F. Zahoor, M. Yousaf, R. Siddique, S. Ahmad, S. A. R. Naqvi and S. M. A. Rizvi, Synthetic strategies toward the synthesis of enoxacin-, levofloxacin-, and gatifloxacin-based compounds: A review, *Synth. Commun.*, 2017, **47**, 1021–1039.
49 N. Kerru, L. Gummidi, S. Maddila, K. K. Gangu and S. B. Jonnalagadda, A review on recent advances in nitrogen-containing molecules and their biological applications, *Molecules*, 2020, **25**, 1909.
50 S. Faiz and A. F. Zahoor, Ring opening of epoxides with C-nucleophiles, *Mol. Diversity*, 2016, **20**, 969–987.
51 P. K. Singh and O. Silakari, The current status of O-heterocycles: A synthetic and medicinal overview, *ChemMedChem*, 2018, **13**, 1071–1087.
52 S. Ahmad, A. F. Zahoor, S. A. R. Naqvi and M. Akash, Recent trends in ring opening of epoxides with sulfur nucleophiles, *Mol. Diversity*, 2018, **22**, 191–205.
53 B. Pathare and T. Bansode, Biological active benzimidazole derivatives, *Results Chem.*, 2021, **3**, 100200.
54 S. S. Garg, J. Gupta, S. Sharma and D. Sahu, D. An insight into the therapeutic applications of coumarin compounds and their mechanisms of action, *Eur. J. Pharm. Sci.*, 2020, **152**, 105424.
55 H. Khanam, Bioactive Benzofuran derivatives: A review, *Eur. J. Med. Chem.*, 2015, **97**, 483–504.
56 B. F. Abdel-Wahab and S. Shaaban, Thiazolothiadiazoles and thiazolooxadiazoles: synthesis and biological applications, *Synthesis*, 2014, **46**, 1709–1716.
57 A. Vaidya, S. Jain, P. Jain, P. Jain, N. Tiwari, R. Jain, R. Jain, A. K. Jain and R. K. K Agrawal, Synthesis and biological activities of oxadiazole derivatives: a review, *Mini-Rev. Med. Chem.*, 2016, **16**, 825–845.
58 A. K. Rathi, R. Syed, H. S. Shin and R. V. Patel, Piperazine derivatives for therapeutic use: a patent review (2010-present), *Expert Opin. Ther. Pat.*, 2016, **26**, 777–797.
59 U. Salma, S. Ahmad, M. Z. Alam and S. A. Khan, A review: Synthetic approaches and biological applications of triazole derivatives, *J. Mol. Struct.*, 2023, **1301**, 137240.
60 S. Koparde, K. M. Hosamani, V. Kulkarni and S. D. Joshi, Synthesis of coumarin-piperazine derivatives as potent anti-microbial and anti-inflammatory agents, and molecular docking studies, *Chem. Data Collect.*, 2018, **15**, 197–206.

61 D. K. Singh, H. Iqbal and M. Ansari, Recent Progress in the Synthesis and Biological Assessment of Benzimidazole-1,2,3-Triazole Hybrids, *Curr. Org. Chem.*, 2024, **28**, 733–756.
62 A. Irfan, S. Faisal, S. Ahmad, S. A. Al-Hussain, S. Javed, A. F. Zahoor, B. Parveen and M. E. Zaki, Structure-based virtual screening of furan-1,3,4-oxadiazole tethered N-phenylacetamide derivatives as novel class of hTYR and hTYRP1 inhibitors, *Pharmaceuticals*, 2023, **16**, 344.
63 A. F. Zahoor, F. Hafeez, A. Mansha, S. Kamal, M. N. Anjum, Z. Raza, S. G. Khan, J. Javid, A. Irfan and M. A. Bhat, Bacterial tyrosinase inhibition, hemolytic and thrombolytic screening, and *in silico* modeling of rationally designed tosyl piperazine-engrafted dithiocarbamate derivatives, *Biomedicines*, 2023, **11**, 2739.
64 S. Saeed, M. J. Saif, A. F. Zahoor, H. Tabassum, S. Kamal, S. Faisal, R. Ashraf, S. G. Khan, U. Nazeer, A. Irfan and M. A. Bhat, Discovery of novel 1, 2, 4-triazole tethered β-hydroxy sulfides as bacterial tyrosinase inhibitors: synthesis and biophysical evaluation through *in vitro* and *in silico* approaches, *RSC Adv.*, 2024, **14**, 15419–15430.
65 R. Kausar, A. F. Zahoor, H. Tabassum, S. Kamal and M. Ahmad Bhat, Synergistic biomedical potential and molecular docking analyses of coumarin–triazole hybrids as tyrosinase inhibitors: design, synthesis, *in vitro* profiling, and *in silico* studies, *Pharmaceuticals*, 2024, **17**, 532.
66 S. Faiz, A. F. Zahoor, M. Ajmal, S. Kamal, S. Ahmad, A. M. Abdelgawad and M. E. Elnaggar, Design, synthesis, antimicrobial evaluation, and laccase catalysis effect of novel benzofuran–oxadiazole and benzofuran–triazole hybrids, *J. Heterocycl. Chem.*, 2019, **56**, 2839–2852.
67 S. B. Ozdemir, Y. U. Cebeci, H. Bayrak, A. Mermer, S. Ceylan, A. Demirbas, S. A. Karoaglu and N. Demirbas, Synthesis and antimicrobial activity of new piperazine-based heterocyclic compounds, *Heterocycl. Commun.*, 2017, **23**, 43–54.
68 S. Saeed, I. Shahzadi, A. F. Zahoor, A. A. Al-Mutairi, S. Kamal, S. Faisal, A. Irfan, S. A. Al-Hussain, M. T. Muhammed and M. E. Zaki, Exploring theophylline-1, 2, 4-triazole tethered N-phenylacetamide derivatives as antimicrobial agents: unraveling mechanisms *via* structure–activity relationship, *in vitro* validation, and *in silico* insights, *Front. Chem.*, 2024, **12**, 1372378.
69 E. A. Elsayed and E. N. Danial, Isolation, Identification and Medium Optimization for Tyrosinase Production by a Newly Isolated *Bacillus subtilis* NA2 Strain, *J. Appl. Pharm. Sci.*, 2018, **8**, 93–101.
70 F. Hussain, S. Kamal, S. Rehman, M. Azeem, I. Bibi, T. Ahmed and H. Iqbal, Alkaline Protease Production Using Response Surface Methodology, Characterization and Industrial Exploitation of Alkaline Protease of *Bacillus subtilis* sp, *Catal. Lett.*, 2017, **147**, 1204–1213.
71 J. H. Kim, J.-Y. Yoon, S. Y. Yang, S.-K. Choi, S. J. Kwon, I. S. Cho, M. H. Jeong, Y. Ho Kim and G. S. Choi, Tyrosinase inhibitory components from Aloevera and their antiviral activity, *J. Enzyme Inhib. Med. Chem.*, 2017, **32**, 78–83.
72 H. Zhong, L. M. Tran and J. L. Stang, Induced-fit Docking Studies of the Active and Inactive States of Protein Tyrosine Ki-nases, *J. Mol. Graphics Modell.*, 2009, **28**, 336–346.
73 W. T. Ismaya, H. J. Rozeboom, A. Weijn, J. J. Mes, F. Fusetti, H. J. Wichers and B. W. Dijkstra, Crystal Structure of Agaricus Bisporus Mushroom Tyrosinase: Identity of the Tetramer Subunits and Interaction with Tropolone, *Biochem.*, 2011, **50**, 5477–5486.
74 L. Fu, S. Shi, J. Yi, N. Wang, Y. He, Z. Wu, J. Peng, Y. Deng, W. Wang, C. Wu, A. Lyu, X. Zeng, W. Zhao, T. Hou and D. Cao, ADMETlab 3.0: an updated comprehensive online ADMET prediction platform enhanced with broader coverage, improved performance, API functionality and decision support, *Nucleic Acids Res.*, 2024, **52**, W422–W431.